

# A constant characteristic volume density of dark matter haloes from SPARC rotation curve fits

Pengfei Li,<sup>1</sup><sup>\*</sup> Federico Lelli,<sup>2</sup><sup>†</sup> Stacy S. McGaugh,<sup>1</sup> Nathaniel Starkman,<sup>1, 3</sup>  
and James M. Schombert<sup>4</sup>

<sup>1</sup>*Department of Astronomy, Case Western Reserve University, Cleveland, OH 44106, USA*

<sup>2</sup>*European Southern Observatory, Karl-Schwarzschild-Strasse 2, Garching bei München, Germany*

<sup>3</sup>*Department of Astronomy and Astrophysics, University of Toronto, Toronto, M5S 3H4 Ontario, Canada*

<sup>4</sup>*Department of Physics, University of Oregon, Eugene, OR 97403, USA*

Accepted XXX. Received YYY; in original form ZZZ

## ABSTRACT

We study the scaling relations between dark matter (DM) haloes and galaxy discs using 175 galaxies from the SPARC database. We explore two cosmologically motivated DM halo profiles: the Einasto profile from DM-only simulations and the DC14 profile from hydrodynamic simulations. We fit the observed rotation curves using a Markov Chain Monte Carlo method and break the disc-halo degeneracy using near-infrared photometry and  $\Lambda$ CDM-motivated priors. We find that the characteristic volume density  $\rho_s$  of DM haloes is nearly constant over  $\sim 5$  decades in galaxy luminosity. The scale radius  $r_s$  and the characteristic surface density  $\rho_s \cdot r_s$ , instead, correlate with galaxy luminosity. These scaling relations provide an empirical benchmark to cosmological simulations of galaxy formation.

**Key words:** dark matter — galaxies: kinematics and dynamics — galaxies: spiral — galaxies: dwarf — galaxies: irregular

## 1 INTRODUCTION

In the cold dark matter (CDM) paradigm, the observed flat rotation curves of disc galaxies (Bosma 1978; Rubin et al. 1978) are attributed to DM haloes. The scaling relations between DM haloes and baryonic discs provide strong constraints to galaxy formation models and have been extensively explored (e.g. van Albada et al. 1985; Kent 1987; de Blok & McGaugh 1997). In particular, Kormendy & Freeman (2004, 2016) collected tens of rotation curve fits with nonsingular isothermal halo profiles and found that the halo central density  $\rho_0$  and core radius  $r_c$  are correlated with galaxy luminosity, while their product  $\rho_0 \cdot r_c$  is nearly a constant. The constancy of  $\rho_0 \cdot r_c$  was also found by Spano et al. (2008) and Donato et al. (2009) using different cored DM halo profiles.

A well-known problem in fitting rotation curves is the disc-halo degeneracy (van Albada et al. 1985): the DM halo parameters are strongly degenerated with the assumed stellar mass-to-light ratio ( $\Upsilon_\star$ ). This can bias the resultant correlations if one does not properly delineate disc and halo contributions to the total rotation curves. In order to break the degeneracy, Kormendy & Freeman (2016) used the

maximum disc method, which is a sensible assumption for high-mass, high-surface-brightness galaxies but could lead to unreasonably high  $\Upsilon_\star$  for low-luminosity, low-surface-brightness galaxies (e.g. Starkman et al. 2018).

The cored DM profiles used in these works are empirically motivated: they often provide good fits to the observed rotation curves. DM-only simulations, however, suggest different profiles. Early N-body simulated haloes were found to be well fit by the NFW profile (Navarro et al. 1996a) which has an inner cusp. This profile, however, does a poor job in fitting the rotation curves of low-luminosity and low-surface-brightness galaxies (e.g. de Blok et al. 2001; de Blok & Bosma 2002; de Blok et al. 2008; Katz et al. 2017). Later simulations with higher resolution showed that the Einasto profile (Einasto 1965) can describe the simulated haloes better than NFW (Navarro et al. 2004; Merritt et al. 2005). This profile, however, has one more parameter and does not consider any baryonic process such as star formation and supernovae feedback which are believed to modify the initial DM distributions (Governato et al. 2010, 2012).

Di Cintio et al. (2014) analysed zoom-in hydrodynamic simulations from the MUGS (Stinson et al. 2010), which consider gas cooling, star formation, and supernovae feedback. They found that the resulting DM density profile at  $z=0$  (hereafter DC14 profile) systematically depends on the

<sup>\*</sup> E-mail: PengfeiLi0606@gmail.com

<sup>†</sup> ESO Fellow

stellar-to-halo mass (SHM) ratio. Thus, simulations with and without baryonic process suggest different halo profiles. It is then of interest to explore the empirical scaling laws for these simulation-based DM profiles.

[Katz et al. \(2017\)](#) use 147 late-type galaxies from the SPARC database ([Lelli et al. 2016](#)) to show that the DC14 profile gives better fits to rotation curves than the NFW profile ([Navarro et al. 1996b](#)). Here we consider the Einasto and DC14 profiles to study scaling laws between DM haloes and baryonic properties of galaxies. Since we consider two cosmologically motivated DM profiles, we can impose  $\Lambda$ CDM priors on halo parameters: the SHM correlation from multi-epoch abundance matching and the mass-concentration (c-M) relation from simulations. The SHM relation can help break the disc-halo degeneracy and the c-M relation breaks the degeneracy between halo parameters. We use homogeneous mass models for 175 galaxies with Spitzer photometry at  $3.6 \mu\text{m}$ , which further help to break the disc-halo degeneracy since  $\Upsilon_\star$  is almost constant in the near infrared (e.g., [McGaugh & Schombert 2014](#); [Meidt et al. 2014](#)).

In Section 2, we introduce the SPARC database, the two halo profiles, and the Bayesian analysis along with the corresponding priors. In Section 3, we show fits of DC14 and Einasto profiles and then present the correlations between DM haloes and galaxy discs. For comparison to [Kormendy & Freeman \(2016\)](#), we also apply the maximum disc method to the pseudo-isothermal profile. We discuss our results in Section 4.

## 2 METHOD

### 2.1 SPARC database

The SPARC database ([Lelli et al. 2016](#)) includes 175 late-type galaxies spanning a wide range in surface brightness (4 dex) and luminosity (5 dex). Their luminosity profiles are well traced by Spitzer photometry at  $3.6 \mu\text{m}$ . According to stellar population synthesis models,  $\Upsilon_\star$  varies little with star formation history of galaxies in near infrared bands (e.g., [McGaugh & Schombert 2014](#); [Meidt et al. 2014](#)). As such, the stellar mass distributions are well determined by Spitzer photometry, providing a physically motivated way to break the disc-halo degeneracy. The wide range in galaxy luminosity, Spitzer photometry in the near infrared band, accurate rotation curves, and relatively large sample make SPARC ideal to explore the properties of DM haloes and their relations to galactic discs.

### 2.2 Halo models

We explore two halo profiles, Einasto and DC14. The Einasto density profile ([Navarro et al. 2004](#)) is given by

$$\rho_{\text{EIN}}(r) = \rho_s \exp \left\{ -\frac{2}{\alpha_\epsilon} \left[ \left( \frac{r}{r_s} \right)^{\alpha_\epsilon} - 1 \right] \right\}, \quad (1)$$

with  $r_s$  the scale radius,  $\rho_s$  the characteristic density and  $\alpha_\epsilon$  describing the rate at which the logarithmic slope decreases towards the center. Its enclosed mass profile ([Mamon & Lokas 2005](#); [Merritt et al. 2006](#)) is given by

$$M(r) = 4\pi\rho_s \exp \left( \frac{2}{\alpha_\epsilon} \right) r_s^3 \left( \frac{2}{\alpha_\epsilon} \right)^{-\frac{3}{\alpha_\epsilon}} \frac{1}{\alpha_\epsilon} \Gamma \left( \frac{3}{\alpha_\epsilon}, \frac{2}{\alpha_\epsilon} \left( \frac{r}{r_s} \right)^{\alpha_\epsilon} \right), \quad (2)$$

where  $\Gamma(a, x) = \int_0^x t^{a-1} e^{-t} dt$  is the incomplete Gamma function.

The DC14 profile is in the form of the  $(\alpha, \beta, \gamma)$  model ([Hernquist 1990](#); [Zhao 1996](#)),

$$\rho(r) = \frac{\rho_s}{\left( \frac{r}{r_s} \right)^\gamma \left[ 1 + \left( \frac{r}{r_s} \right)^\alpha \right]^{(\beta-\gamma)/\alpha}}, \quad (3)$$

where  $\beta$  defines the outer slope,  $\gamma$  the inner slope, and  $\alpha$  measures the width of the transition region. The values of these parameters depend on the SHM ratio:

$$\begin{aligned} \alpha &= 2.94 - \log[(10^{X+2.33})^{-1.08} + (10^{X+2.33})^{2.29}], \\ \beta &= 4.23 + 1.34X + 0.26X^2, \\ \gamma &= -0.06 + \log[(10^{X+2.56})^{-0.68} + 10^{X+2.56}], \end{aligned} \quad (4)$$

where  $X = \log(M_\star/M_{\text{halo}})$  is the logarithmic SHM ratio,  $M_\star$  is the stellar mass, and  $M_{\text{halo}}$  is the total halo mass. For  $X < -4.1$ , the profile returns to the NFW form since there is not enough energy from supernovae to substantially modify the halo profile. For  $X > -1.3$ , feedback from active galactic nuclei is expected to be important and the DC14 profile may not be an effective description any more since it takes only stellar feedback into account. Following [Katz et al. \(2017\)](#), we consider  $X = -1.3$  as the highest possible value for SPARC galaxies. With the constraints of equation 4, the DC14 halo has only two free parameters. Its enclosed mass within radius  $r$  can be calculated by changing the variable from  $r$  to

$$\epsilon = \frac{(r/r_s)^\alpha}{1 + (r/r_s)^\alpha} \quad (5)$$

so that

$$M(r) = 4\pi r_s^3 \rho_s \frac{1}{\alpha} [B(a, b+1, \epsilon) + B(a+1, b, \epsilon)], \quad (6)$$

where  $B(a, b, x) = \int_0^x t^{a-1} (1-t)^{b-1} dt$  is the incomplete Beta function,  $a = (3-\gamma)/\alpha$  and  $b = (\beta-3)/\alpha$ .

We define the dimensionless radius  $x = r/r_s$  and adopt the virial radius  $r_{200}$  inside of which the average density is 200 times the critical density of the universe ( $\rho_{\text{crit}} = \frac{3H_0^2}{8\pi G}$ ). We also define  $M_{\text{halo}}$  as the total mass within their virial radius. The concentration  $C_{200}$  and the rotation velocity  $V_{200}$  at the virial radius are then given by

$$C_{200} = r_{200}/r_s, \quad V_{200} = 10 C_{200} r_s H_0, \quad (7)$$

where  $H_0$  is the Hubble constant ( $73 \text{ km s}^{-1} \text{ Mpc}^{-1}$  in this paper).

With these notations, the rotation velocity from DM haloes is given by

$$\frac{V_{\text{Ein}}}{V_{200}} = \sqrt{\frac{C_{200}}{x} \frac{\Gamma(\frac{3}{\alpha_\epsilon}, \frac{2}{\alpha_\epsilon} x^{\alpha_\epsilon})}{\Gamma(\frac{3}{\alpha_\epsilon}, \frac{2}{\alpha_\epsilon} C_{200}^{\alpha_\epsilon})}}, \quad (8)$$

$$\frac{V_{\text{DC14}}}{V_{200}} = \sqrt{\frac{C_{200}}{x} \frac{B(a, b+1, \epsilon) + B(a+1, b, \epsilon)}{B(a, b+1, \epsilon_c) + B(a+1, b, \epsilon_c)}}, \quad (9)$$

where  $\epsilon_c = \frac{C_{200}^\alpha}{1+C_{200}^\alpha}$ . The total rotational velocity is given by

$$V_{\text{tot}}^2 = V_{\text{DM}}^2 + \Upsilon_{\text{disc}} V_{\text{disc}}^2 + \Upsilon_{\text{bul}} V_{\text{bul}}^2 + V_{\text{gas}}^2, \quad (10)$$

where  $V_{\text{disc}}$ ,  $V_{\text{bul}}$  and  $V_{\text{gas}}$  are the contributions of disc, bulge and gas, respectively, as tabulated in the SPARC database ([Lelli et al. 2016](#)).  $\Upsilon_{\text{disc}}$  and  $\Upsilon_{\text{bul}}$  are the stellar mass-to-light

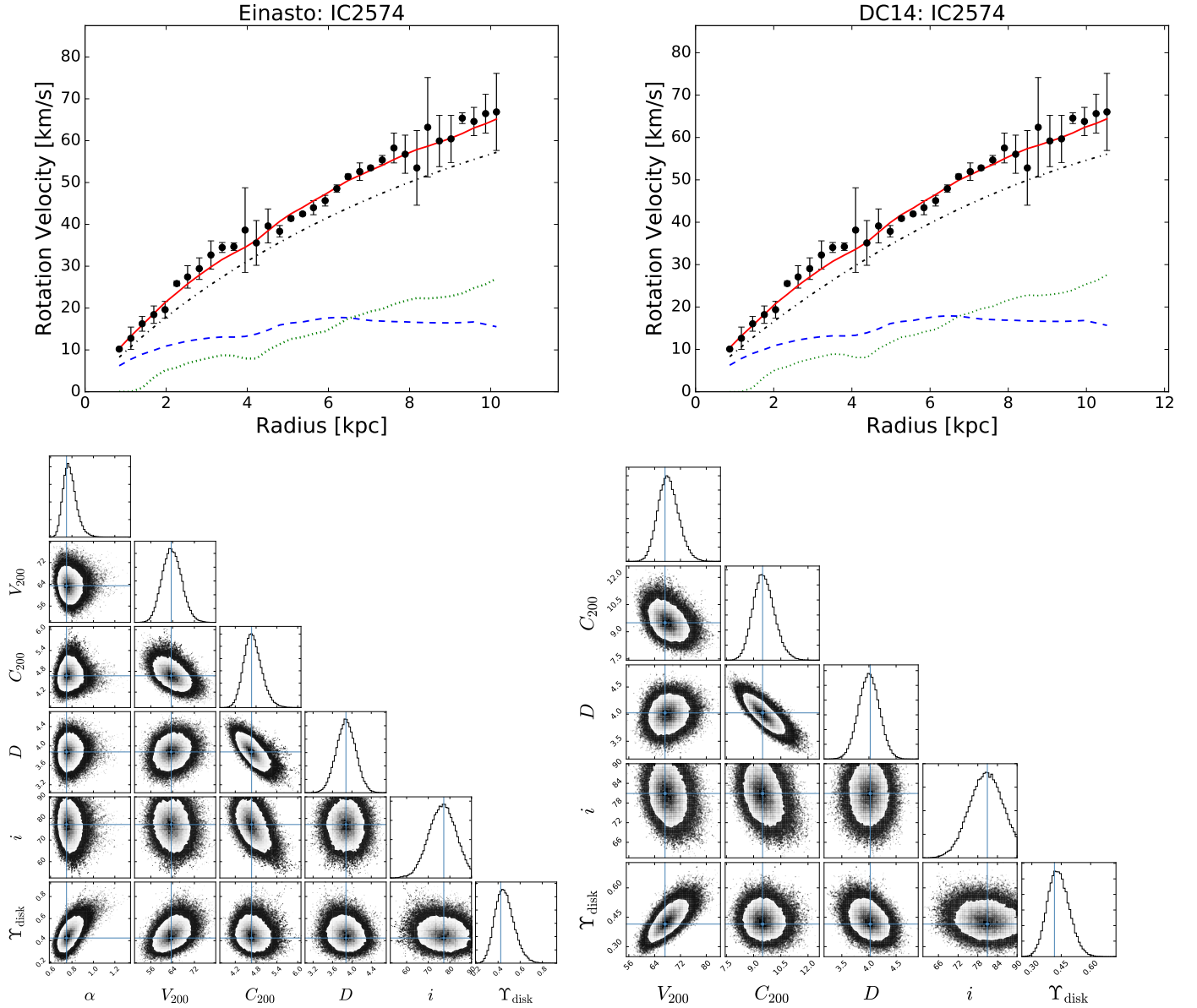


**Figure 1.** Rotation curve fits and posterior distributions of fitting parameters for the dwarf galaxy IC2574 using Einasto (left) and DC14 (right) profiles. Green, blue and black lines show the contributions of gas, disc and dark matter, respectively. Red lines represent the total fitted rotation curves. The complete figure set of 175 images is available at the [SPARC website](#).

ratios of disc and bulge with fiducial values of 0.5 and 0.7, respectively.

As described in Li et al. (2018), galaxy distance ( $D$ ) and disc inclination ( $i$ ) affect the stellar components and the total observed rotational velocities ( $V_{\text{obs}}$ ), respectively. They transform as

$$V'_k = V_k \sqrt{\frac{D'}{D}}, \quad V'_{\text{obs}} = V_{\text{obs}} \frac{\sin(i)}{\sin(i')}, \quad (11)$$

where  $k$  denotes disc, bulge or gas, respectively. We allow  $D$  and  $i$  to vary by imposing Gaussian priors with standard deviations given by the observational errors. Thus, the free parameters in our fits are totally fixed by  $\Upsilon_{\star}$ ,  $D$ ,  $i$ ,  $V_{200}$ ,  $C_{200}$  and additionally  $\alpha_{\epsilon}$  for the Einasto model.

### 2.3 Bayesian analysis

For both Einasto and DC14 models, we map the posterior distributions of halo parameters, as well as the three galactic parameters ( $\Upsilon_{\star}$ ,  $D$ ,  $i$ ) using the open source Python package *emcee* (Foreman-Mackey et al. 2013). In Bayesian analysis, posterior distributions are determined by priors and likelihood functions. The latter is chosen as  $\exp(-\frac{1}{2}\chi^2)$  in which  $\chi^2$  is defined in terms of rotational velocities,

$$\chi^2 = \sum_R \frac{[V_{\text{obs}}(R) - V_{\text{tot}}(R)]^2}{(\delta V_{\text{obs}})^2}, \quad (12)$$

where  $\delta V_{\text{obs}}$  is the uncertainty on rotational velocities. We impose the same priors on galactic parameter as in Li et al. (2018): Gaussian priors on  $D$  and  $i$  around their tabulated

values in the SPARC database with standard deviations given by the observational errors; lognormal prior on  $\Upsilon_{\star}$  around their fiducial values  $\Upsilon_{\text{disc}} = 0.5$  and  $\Upsilon_{\text{bul}} = 0.7$  with a standard deviation of 0.1 dex suggested by stellar population synthesis models (McGaugh et al. 2016; Lelli et al. 2017).

We set loose boundaries on halo parameters:  $10 < V_{200} < 500$  km/s,  $0 < C_{200} < 100$  for Einasto and DC14 models, and  $0 < \alpha_{\epsilon} < 2$  for Einasto. We obtain one set of fits with flat priors on halo parameters and another one with  $\Lambda$ CDM priors, comprising the SHM and mass-concentration relations.

The SHM relation (Moster et al. 2013) presents a lognormal distribution around the mean relation,

$$\frac{M_{\star}}{M_{\text{halo}}} = 2N \left[ \left( \frac{M_{\text{halo}}}{M_1} \right)^{-\beta} + \left( \frac{M_{\text{halo}}}{M_1} \right)^{\gamma} \right]^{-1}, \quad (13)$$

with a scatter of  $\sigma(\log M_{\star}) = 0.15$  dex. The parameters in the equation are fixed by multi-epoch abundance matching:  $\log(M_1) = 11.59$ ,  $N = 0.0351$ ,  $\beta = 1.376$  and  $\gamma = 0.608$ .

Halo concentrations and halo masses are found to follow a power law (Macciò et al. 2008),

$$\log(C_{200}) = a - b \log(M_{\text{halo}}/[10^{12} h^{-1} M_{\odot}]), \quad (14)$$

with an intrinsic scatter of 0.11 dex. The parameter  $a$  and  $b$  depend on cosmology and adopted DM profiles. Macciò et al. (2008) gives specific relations in different cosmologies. We adopt the values corresponding to the *WMAP5* cosmology (equation 10 in Macciò et al. 2008), which gives  $a = 0.830$  and  $b = -0.098$  for DC14. For the Einasto model, the only available results are for the *Planck* cosmology (Dutton & Macciò 2014):  $a = 0.977$  and  $b = -0.130$ . In the SPARC database, the distances of some galaxies are estimated with flow models assuming  $H_0 = 73$  km s $^{-1}$  Mpc $^{-1}$ . This is consistent with the local distance scale (Tully et al. 2016; Riess et al. 2016) but is not entirely consistent with either cosmology. Flow distances have large errors, so this small inconsistency plays a very minor role and only affect the final values of the best-fit distances.

For the extra parameter  $\alpha_{\epsilon}$  in the Einasto model, Dutton & Macciò (2014) shows that its value depends on halo mass,

$$\alpha = 0.0095v^2 + 0.155, \quad (15)$$

where  $\log v = -0.11 + 0.146m + 0.0138m^2 + 0.00123m^3$  and  $m = \log(M_{\text{halo}}/10^{12} h^{-1} M_{\odot})$ . The measured standard deviation in their simulation is 0.16 dex around the above relation. This constraint is important. Left free,  $\alpha$  can mimic a constant density core. This can provide good fits to rotation curves, but is not consistent with  $\Lambda$ CDM (Chemin et al. 2011).

The above relations compose the  $\Lambda$ CDM priors. We then use the standard affine-invariant ensemble sampler in *emcee* to map the posterior distributions based on the above likelihood function for both flat and  $\Lambda$ CDM priors.

## 3 RESULTS

### 3.1 Individual fits

In Figure 1, we show an example fit for a gas-dominated dwarf galaxy (IC 2574). The best-fit parameters of these two profiles are close, except that Einasto prefers a smaller

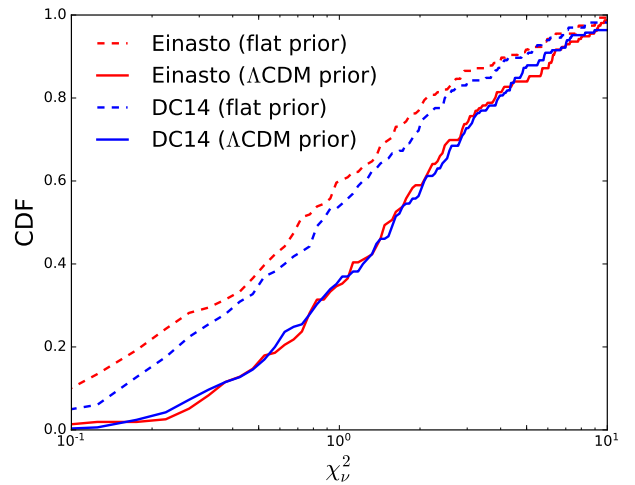


**Figure 2.** The cumulative distributions of  $\chi_v^2$  for Einasto (red lines) and DC14 (blue lines) models imposing flat priors (solid lines) and  $\Lambda$ CDM priors (dashed lines).

concentration than does DC14. This is a general trend for SPARC galaxies, which is due to the large values of  $\alpha_{\epsilon}$  as shown in Figure A4. For IC2574,  $\alpha_{\epsilon} = 0.76$ . This is larger than the expectation of the imposed  $\Lambda$ CDM prior. This is a manifestation of the cusp-core problem: the fits frequently prefer  $\alpha_{\epsilon}$  that are more consistent with a cored DM halo profile.

### 3.2 Fit goodness

To check the fit quality of Einasto and DC14 models, we inspect the cumulative distribution functions (CDF) of their  $\chi_v^2$  for both flat and  $\Lambda$ CDM priors (Figure 2). Flat priors give better fits than  $\Lambda$ CDM priors due to the weaker constraints on the free parameters. The resulting best-fit values, however, do not necessarily agree with the expectations from  $\Lambda$ CDM cosmological simulations. For example, for flat priors, although the Einasto profile gives better fits to SPARC galaxies than DC14, its shape parameter  $\alpha_{\epsilon}$  is systematically higher than expected (see Figure A4). In general, we explore flat priors just to check the maximum ability of a model to fit real galaxies.

When the  $\Lambda$ CDM priors are imposed, Einasto and DC14 models show comparable fit quality, but Einasto is making use of an additional parameter. In the appendix, we show the distributions of galactic parameters and check how well the  $\Lambda$ CDM priors are recovered. We also check that the SHM ratios for both models are in the range of  $[-3.5, -0.5]$  for SPARC galaxies, thereby allowing sufficient stellar feedback. The resultant  $\chi_v^2$  do not correlate with SHM ratios, indicating neither model introduces any systematics. Since both profiles can describe the data comparably well, we proceed to explore possible disc-halo correlations.

### 3.3 Correlations between halo and disc properties

In Figure 3, we plot  $r_s$  (top panels),  $\rho_s$  (middle panels) and  $\rho_s \cdot r_s$  (bottom panels) against the observed luminosity at

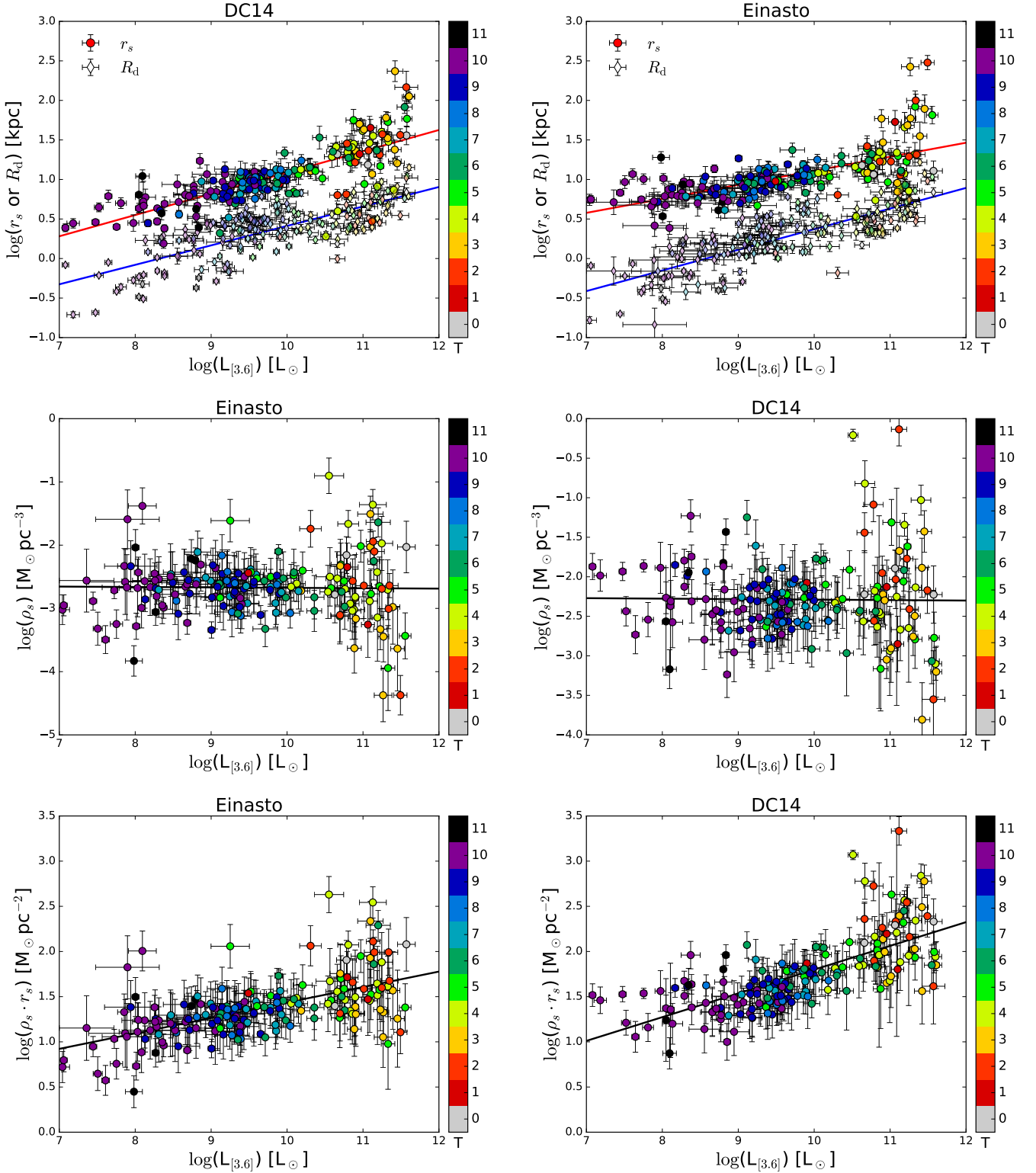


**Figure 3.** Scaling relations between halo properties and galaxy [3.6] luminosity for Einasto (left) and DC14 (right) profiles when imposing  $\Lambda$ CDM priors. Top: halo scale radius and disc scale length. Middle: halo characteristic volume density  $\rho_s$ . Bottom: halo characteristic surface density  $\rho_s \cdot r_s$ . Galaxies are colour-coded by Hubble type with numbers from 0 to 11 corresponding to S0, Sa, Sab, Sb, Sbc, Sc, Scd, Sd, Sdm, Sm, Im, BCD, respectively. In all panels, solid lines show linear fits.



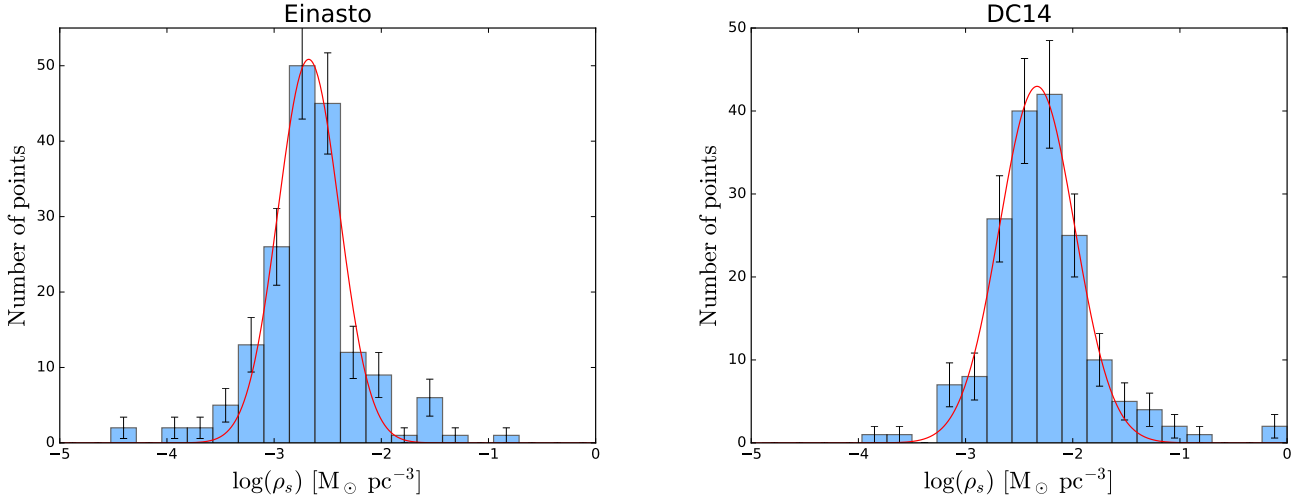


**Figure 4.** Histograms of the best-fit values of  $\rho_s$  for Einasto and DC14 profiles. Red lines are fitted Gaussian functions.

**Table 1.** The slopes of the fitted linear relations for  $R_d$ ,  $r_s$  and  $\rho_s \cdot r_s$  against galaxy luminosity  $L_{[3.6]}$  in log space.

Model	$R_d$	$r_s$	$\rho_s \cdot r_s$
Einasto	$0.26 \pm 0.01$	$0.18 \pm 0.02$	$0.17 \pm 0.02$
DC14	$0.25 \pm 0.02$	$0.27 \pm 0.02$	$0.26 \pm 0.02$

[3.6] when imposing  $\Lambda$ CDM priors. In the top panels, we also show the relation with the disc scale length  $R_d$ , which is obtained by fitting an exponential profile to the outer parts of the [3.6] luminosity profile (see Lelli et al. 2016 for details). Both galaxy luminosity and disc scale length from the SPARC database are converted to the new best-fit distances. The uncertainty in  $R_d$  is dominated by the error in distance. The uncertainty in  $L_{[3.6]}$  is the quadratic sum of errors on distances and flux as tabulated in SPARC. We calculate errors on  $r_s$  and  $\rho_s \cdot r_s$  by error propagation based on the uncertainties in the fitting parameters.

In the top panels, both  $r_s$  and  $R_d$  show an apparent correlation with galaxy luminosity. To quantify the strength of these correlations, we calculate their Pearson  $r$  coefficient and find,  $r(r_s) = 0.65$ ,  $r(R_d) = 0.81$  for Einasto and  $r(r_s) = r(R_d) = 0.77$  for DC14, indicating strong correlations. We fit the data to a linear relation in log-space:

$$\begin{aligned} \log r_s &= (0.18 \pm 0.02) \log L_{[3.6]} - (0.67 \pm 0.15), \\ \log R_d &= (0.26 \pm 0.01) \log L_{[3.6]} - (2.24 \pm 0.14) \end{aligned} \quad (16)$$

for Einasto and

$$\begin{aligned} \log r_s &= (0.27 \pm 0.02) \log L_{[3.6]} - (1.6 \pm 0.17), \\ \log R_d &= (0.25 \pm 0.02) \log L_{[3.6]} - (2.05 \pm 0.15) \end{aligned} \quad (17)$$

for DC14 as shown in Table A2 and A2. Although Einasto and DC14 show different power laws in halo scale radius, they almost share the same correlation between  $R_d$  and  $L_{[3.6]}$ . Lelli et al. (2016) show the correlation between the original values of  $R_d$  and  $L_{[3.6]}$  (their Figure 2). We check the power index is about 0.25, consistent with our results.

The bottom panels of Figure 3 shows that  $\rho_s \cdot r_s$  correlates with galaxy luminosity: their Pearson  $r$  values for

Einasto and DC14 are 0.59 and 0.70, respectively. The fitted power laws are

$$\log \rho_s \cdot r_s = (0.17 \pm 0.02) \log L_{[3.6]} - (0.28 \pm 0.17) \quad (18)$$

for Einasto and

$$\log \rho_s \cdot r_s = (0.26 \pm 0.02) \log L_{[3.6]} - (0.83 \pm 0.20) \quad (19)$$

for DC14. These strong correlations are in contrast with what Kormendy & Freeman (2016) found: a roughly constant central surface density,  $\rho_0 \cdot r_c \propto L_B^{0.058 \pm 0.067}$ . We note, however, that the product  $\rho_s \cdot r_s$  has a different meaning from  $\rho_0 \cdot r_c$  in Kormendy & Freeman (2016) as they use a different halo model. The constant central density of their non-singular isothermal halo contrasts with the variable inner density profile of the Einasto and DC14 halo models. This issue is further discussed in the next Section.

Remarkably,  $r_s$  and  $\rho_s \cdot r_s$  correlate with galaxy luminosity with the same power law for both halo profiles. This suggests that the characteristic volume density  $\rho_s$  is almost constant. This is evident from the middle panels of Figure 3. The Pearson  $r$  products indeed are negligible ( $\sim -0.01$ ) for both profiles. The best-fit relations are almost flat with  $\log(\rho_s) = -2.7 \pm 0.3$  [ $M_\odot \text{pc}^{-3}$ ] for Einasto and  $\log(\rho_s) = -2.3 \pm 0.1$  [ $M_\odot \text{pc}^{-3}$ ] for DC14. Since our fits recover a tight stellar-to-halo mass relation (see Figure A3), it is clear that  $\rho_s$  does not correlate with halo mass either.

We colour-code galaxies by Hubble type in all panels of Figure 3. The well-known correlation of galaxy type with luminosity is obvious. We see no evidence for a dependence of halo parameters on morphological type beyond the variation with luminosity (cf. Korsaga et al. 2018a,b).

Figure 4 shows the histograms of the volume density parameter  $\rho_s$  for both profiles. Despite the limited statistics, they roughly show Gaussian shapes. We fit their distributions to Gaussian functions (red lines). The fitted Gaussian profiles have mean values of -2.7 and -2.3 for Einasto and DC14, respectively, consistent with the fitted linear relations. Their corresponding standard deviations are  $\sigma(\text{Einasto}) = 0.29 \pm 0.02$  dex and  $\sigma(\text{DC14}) = 0.35 \pm 0.01$

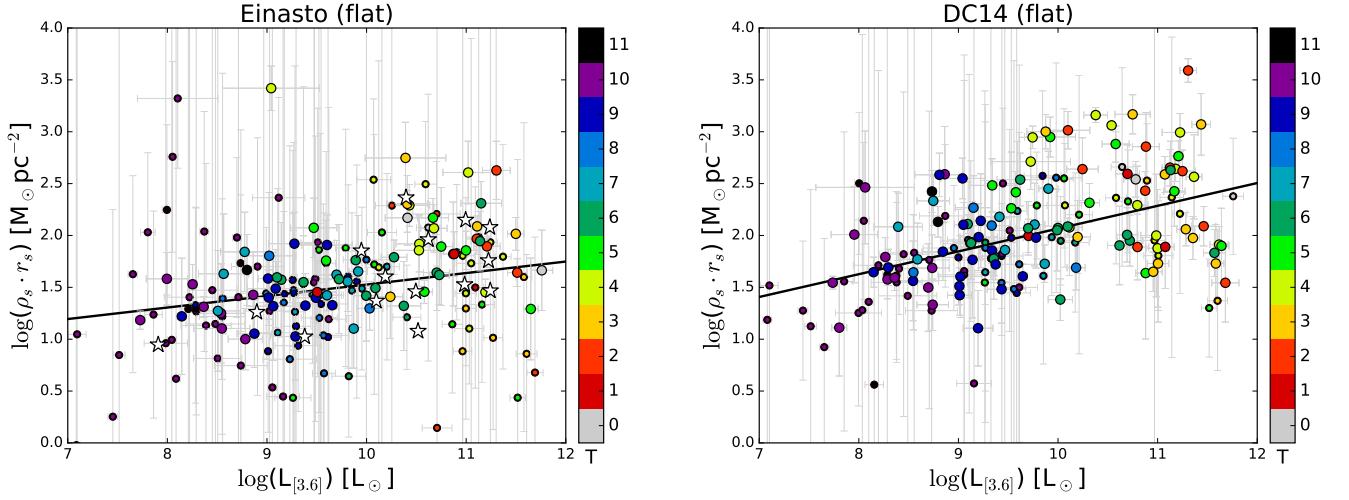


**Figure 5.** The product  $\rho_0 \cdot r_s$  vs. galaxy luminosity for both profiles when imposing flat priors. Galaxies are colour-coded by Hubble type. Solid lines are the best-fit linear relations. Large and small points represent galaxies with uncertainties on  $r_s$  smaller and larger than 20%, respectively. White stars on the left panel are the fit results from Chemin et al. (2011) using the same halo profile.

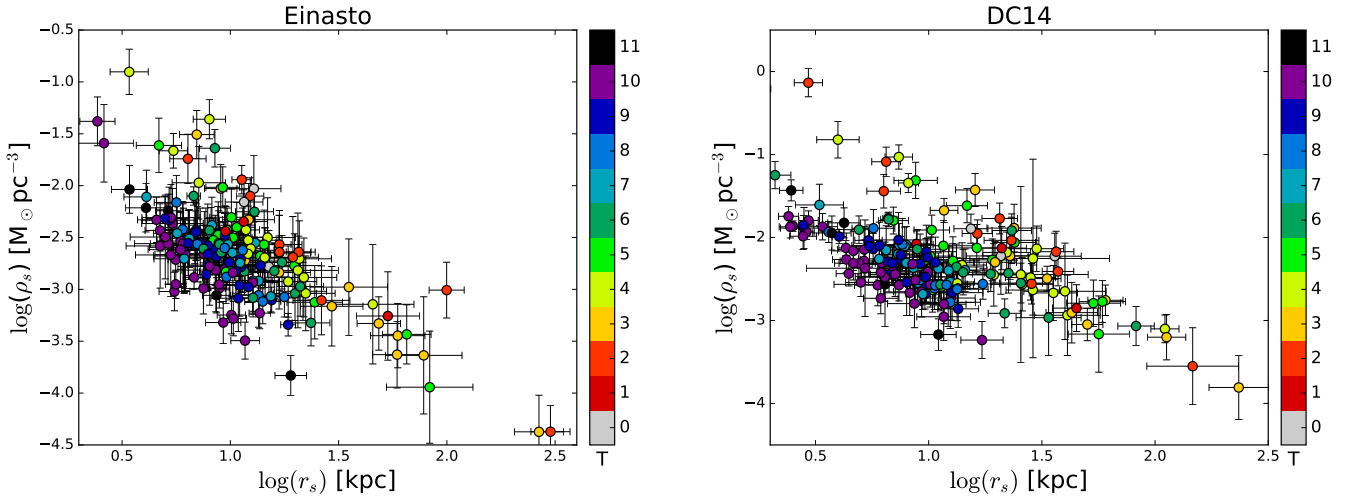


**Figure 6.** Characteristic volume density  $\rho_s$  is plotted against scale radius  $r_s$  in log space for the Einasto (left) and DC14 (right) profiles when imposing  $\Lambda$ CDM priors. Galaxies are color-coded by Hubble type.

dex. These are smaller than the rms scatter (0.48 dex for Einasto and 0.50 dex for DC14) due to outliers.

In Figure 5, we plot  $\rho_s \cdot r_s$  against galaxy luminosity when imposing a flat rather than Gaussian prior. The fitted solid lines for both profiles still show correlations with galaxy luminosity, but with significantly larger scatter. The degeneracy between  $\rho_s$  and  $r_s$  increases the uncertainties on  $\rho_s \cdot r_s$  dramatically for both models. Thus, before we can make claims about the constancy (or lack thereof) of the product  $\rho_s \cdot r_s$ , the degeneracy must be broken.

A detailed study of the Einasto profile was performed by Chemin et al. (2011) fitting 17 rotation curves from the THINGS survey (Walter et al. 2008; de Blok et al. 2008). When using a Kroupa IMF (Kroupa 2001), their values of  $\Upsilon_\star$  are around 0.5, which is consistent with our stellar popu-

lation synthesis prior. In the left panel of Figure 5, we overplot their results (from their Table 2) as white stars. The SPARC sample is about one order of magnitude larger than that in Chemin et al. (2011), so our scaling relations are better defined.

The relation between the halo parameters  $\rho_s$  and  $r_s$  themselves are shown in Figure 6. Similar relations were explored before using smaller galaxy samples (e.g., Chemin et al. 2011; Kormendy & Freeman 2016). Figure 6 shows that late-type and early-type disc galaxies cover distinct regions in the  $r_s - \rho_s$  plane: late-type galaxies (Sd to Im) tend to have lower halo densities at a given  $r_s$  than early-type spirals (S0 to Sc). Late-type galaxies have, on average, lower surface brightness than early-type galaxies (e.g. Lelli et al. 2016), so Figure 6 suggests that low-surface-brightness

galaxies may inhabit lower density haloes than high-surface-brightness galaxies (de Blok & McGaugh 1996; McGaugh & de Blok 1998). The data are consistent with a trend of increasing  $r_s$  with decreasing  $\rho_s$ , but we refrain from fitting power-laws because the trend is driven by a few extreme objects, and may depend systematically on morphological type. For the Einasto profile, we also investigated the relations between  $\alpha_\epsilon$  and the other halo parameters, finding no significant correlation with either  $\rho_s$  or  $r_s$ .

#### 4 COMPARISON WITH PREVIOUS WORK

The correlation between  $\rho_s \cdot r_s$  and galaxy luminosity seems to contradict the constant  $\rho_0 \cdot r_c$  found in previous studies (Spano et al. 2008; Donato et al. 2009; Kormendy & Freeman 2016). However, these two quantities are not exactly the same, since  $\rho_0$  is the central volume density of cored DM halo profiles, while  $\rho_s$  is the characteristic volume density of the Einasto or DC14 profiles. Moreover, we use different analysis methods.

To break the disc-halo degeneracy, Spano et al. (2008) assume constant  $\Upsilon_\star$  at  $R$  band, but stellar population synthesis models predict strong variation of  $\Upsilon_\star$  in optical bands (e.g. McGaugh & Schombert 2014). Donato et al. (2009) delineated stellar contributions using a mixture of methods such as fitting the universal rotation curve (Persic et al. 1996) and adopting spectro-photometric galaxy models. Thus, the contributions of each component strongly depend on the efficacy of the modelling. Kormendy & Freeman (2016) adopt the maximum disc method, which may be unphysical for low-mass and low surface-brightness galaxies (e.g. Starkman et al. 2018). Moreover, all these studies assume flat priors on the halo parameters. As we showed in the previous Section, flat priors can significantly blur the  $\rho_s \cdot r_s$  correlation with galaxy luminosity. In the following, we show that the method to break the disc-halo degeneracy also makes a big difference.

To understand the origin of these different results, we employ the maximum disc method and fit the pseudo-isothermal (pISO) profile,

$$\rho(r) = \rho_0 [1 + (r/r_0)^2]^{-1} \quad (20)$$

where  $\rho_0 \cdot r_0$  has the meaning of central surface density. To implement the maximum disc method, we adopt the maximum disc values of  $\Upsilon_\star$  from Starkman et al. (2018). For consistency, we fix galaxy distances and disc inclinations to the original values from the SPARC database. Therefore, the only fitting parameters are those on DM haloes. For better comparison with Kormendy & Freeman (2016), we impose flat priors on halo parameters.

The resultant  $\rho_0 \cdot r_0$  against galaxy luminosity is shown in Figure 7. The correlation between  $\rho_0 \cdot r_0$  and galaxy luminosity is pretty weak: its Pearson  $r$  value is 0.16. The fitted line has a slope of  $0.075 \pm 0.035$ , consistent with that of Kormendy & Freeman (2016). Thus, we obtain the same result when we make comparable assumptions about the disc and halo.

The maximum disc method gives a different result from our population synthesis result. According to the correlations shown in the previous section, more luminous galaxies tend to have larger  $r_s$  and  $\rho_s \cdot r_s$  while leaving  $\rho_s$  almost

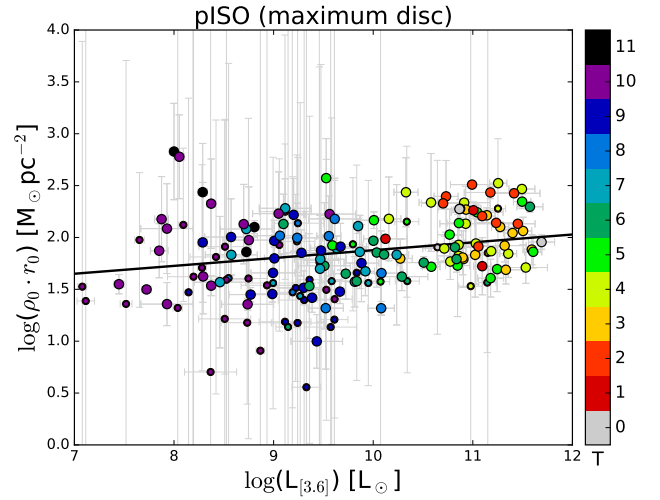


**Figure 7.** Same as Figure 5 but for pISO profile with the maximum disc method.

constant. However, the maximum disc method makes stellar discs to contribute as much as they can, which compensates the contribution from DM haloes. It hence leads to a constant central surface density ( $\rho_0 \cdot r_0$ ) of dark matter. Our result differs because of the different prior on  $\Upsilon_{\text{disc}}$ , not because of any conflict in the data. The maximum disc method pushes the  $\Upsilon_{\text{disc}}$  for low-mass galaxies to unreasonably high values, so this prior seems less physical than the population synthesis prior.

#### 5 CONCLUSIONS

In this paper, we fit SPARC galaxy rotation curves with two simulation-motivated profiles (Einasto and DC14) and show that the properties of DM haloes and stellar discs are strongly correlated. However, the characteristic volume density  $\rho_s$  is constant over 5 dex in luminosity for both profiles. Although different galaxies show quite different rotation curves, they consistently require constant  $\rho_s$ .

The constant volume density provides new insights into galaxy formation. It indicates that halo volume density is unrelated to galaxy luminosity. In the  $\Lambda$ CDM context, more luminous galaxies must be hosted in bigger haloes, but the halo size and mass must progressively increase in order to keep the characteristic volume density constant. It would be interesting to see whether this phenomenology is reproduced in cosmological simulations of galaxy formation. Presumably, the characteristic volume density of DM haloes depend on the implementation of baryonic physics (star formation, stellar feedback, etc.), so our scaling relations provide crucial benchmarks for theories of galaxy formation.

#### ACKNOWLEDGMENTS

This work is based in part on observations made with the Spitzer Space Telescope, which is operated by the Jet Propulsion Laboratory, California Institute of Technology under a contract with NASA.



## REFERENCES

- Bosma A., 1978, PhD thesis, PhD Thesis, Groningen Univ., (1978)
- Chemin L., de Blok W. J. G., Mamon G. A., 2011, *AJ*, **142**, 109
- Di Cintio A., Brook C. B., Dutton A. A., Macciò A. V., Stinson G. S., Knebe A., 2014, *MNRAS*, **441**, 2986
- Donato F., et al., 2009, *MNRAS*, **397**, 1169
- Dutton A. A., Macciò A. V., 2014, *MNRAS*, **441**, 3359
- Einasto J., 1965, Trudy Astrofizicheskogo Instituta Alma-Ata, **5**, 87
- Foreman-Mackey D., Hogg D. W., Lang D., Goodman J., 2013, *PASP*, **125**, 306
- Governato F., et al., 2010, *Nature*, **463**, 203
- Governato F., et al., 2012, *MNRAS*, **422**, 1231
- Hernquist L., 1990, *ApJ*, **356**, 359
- Katz H., Lelli F., McGaugh S. S., Di Cintio A., Brook C. B., Schombert J. M., 2017, *MNRAS*, **466**, 1648
- Kent S. M., 1987, *AJ*, **93**, 816
- Kormendy J., Freeman K. C., 2004, in Ryder S., Pisano D., Walker M., Freeman K., eds, IAU Symposium Vol. 220, Dark Matter in Galaxies. p. 377 ([arXiv:astro-ph/0407321](https://arxiv.org/abs/astro-ph/0407321))
- Kormendy J., Freeman K. C., 2016, *ApJ*, **817**, 84
- Korsaga M., Amram P., Carignan C., Epinat B., 2018a, preprint, ([arXiv:1809.06306](https://arxiv.org/abs/1809.06306))
- Korsaga M., Carignan C., Amram P., Epinat B., Jarrett T. H., 2018b, *MNRAS*, **478**, 50
- Kroupa P., 2001, *MNRAS*, **322**, 231
- Lelli F., McGaugh S. S., Schombert J. M., 2016, *AJ*, **152**, 157
- Lelli F., McGaugh S. S., Schombert J. M., Pawlowski M. S., 2017, *ApJ*, **836**, 152
- Li P., Lelli F., McGaugh S., Schombert J., 2018, *A&A*, **615**, A3
- Macciò A. V., Dutton A. A., van den Bosch F. C., 2008, *MNRAS*, **391**, 1940
- Mamon G. A., Lokas E. L., 2005, *MNRAS*, **362**, 95
- McGaugh S. S., Schombert J. M., 2014, *AJ*, **148**, 77
- McGaugh S. S., de Blok W. J. G., 1998, *ApJ*, **499**, 41
- McGaugh S. S., Lelli F., Schombert J. M., 2016, *Physical Review Letters*, **117**, 201101
- Meidt S. E., et al., 2014, *ApJ*, **788**, 144
- Merritt D., Navarro J. F., Ludlow A., Jenkins A., 2005, *ApJ*, **624**, L85
- Merritt D., Graham A. W., Moore B., Diemand J., Terzić B., 2006, *AJ*, **132**, 2685
- Mozer B. P., Naab T., White S. D. M., 2013, *MNRAS*, **428**, 3121
- Navarro J. F., Eke V. R., Frenk C. S., 1996a, *MNRAS*, **283**, L72
- Navarro J. F., Frenk C. S., White S. D. M., 1996b, *ApJ*, **462**, 563
- Navarro J. F., et al., 2004, *MNRAS*, **349**, 1039
- Navarro J. F., et al., 2010, *MNRAS*, **402**, 21
- Persic M., Salucci P., Stel F., 1996, *MNRAS*, **281**, 27
- Riess A. G., et al., 2016, *ApJ*, **826**, 56
- Rubin V. C., Ford Jr. W. K., Thonnard N., 1978, *ApJ*, **225**, L107
- Spano M., Marcelin M., Amram P., Carignan C., Epinat B., Hernandez O., 2008, *MNRAS*, **383**, 297
- Starkman N., Lelli F., McGaugh S., Schombert J., 2018, *MNRAS*, **480**, 2292
- Stinson G. S., Bailin J., Couchman H., Wadsley J., Shen S., Nickerson S., Brook C., Quinn T., 2010, *MNRAS*, **408**, 812
- Tissera P. B., White S. D. M., Pedrosa S., Scannapieco C., 2010, *MNRAS*, **406**, 922
- Tully R. B., Courtois H. M., Sorce J. G., 2016, *AJ*, **152**, 50
- Walter F., Brinks E., de Blok W. J. G., Bigiel F., Kennicutt Jr. R. C., Thornley M. D., Leroy A., 2008, *AJ*, **136**, 2563
- Zhao H., 1996, *MNRAS*, **278**, 488
- de Blok W. J. G., Bosma A., 2002, *A&A*, **385**, 816
- de Blok W. J. G., McGaugh S. S., 1996, *ApJ*, **469**, L89
- de Blok W. J. G., McGaugh S. S., 1997, *MNRAS*, **290**, 533
- de Blok W. J. G., McGaugh S. S., Bosma A., Rubin V. C., 2001, *ApJ*, **552**, L23
- de Blok W. J. G., Walter F., Brinks E., Trachternach C., Oh S.-H., Kennicutt Jr. R. C., 2008, *AJ*, **136**, 2648
- van Albada T. S., Bahcall J. N., Begeman K., Sancisi R., 1985, *ApJ*, **295**, 305

APPENDIX A: CHECKING THE DISTRIBUTIONS OF GALACTIC PARAMETERS AND  $\Lambda$ CDM PRIORS

## A1 Distributions of galactic parameters

We plot the distributions of optimized galactic parameters for Einasto and DC14 models in Figure A1 and A2, respectively. The distributions of  $\Upsilon_{\star}$  are shown in the top panels for both models. Red dashed lines indicate their fiducial values ( $\Upsilon_{\text{disc}} = 0.5$  and  $\Upsilon_{\text{bul}} = 0.7$  according to [McGaugh et al. 2016](#)). We check that the median values of the optimized  $\Upsilon_{\text{disc}}$  for Einasto and DC14 are close to the fiducial value: 0.49 for Einasto and 0.52 for DC14. Einasto clearly shows a tighter distribution than DC14. There are 32 galaxies in the SPARC database hosting a bulge and the distributions of their optimized  $\Upsilon_{\text{bul}}$  are shown in top-right panels. Their median values for both models are slightly smaller than the fiducial value: 0.63 for Einasto and 0.58 for DC14.

In the bottom panels, adjusted distances and inclinations are plotted against their original values as tabulated in the SPARC database. Errors on the adjusted values are calculated by the output of ‘std’ in the open software ‘GetDist’. Distances of SPARC galaxies are measured with five different methods: the Hubble flow corrected for Virgo-centric infall, the tip of the red giant branch (TRGB) method, the magnitude-period relation of Cepheids, membership to the Ursa Major cluster of galaxies (UMA cluster), and supernovae (SN) light curves. Hubble flow is the least accurate method, hence the corresponding distances present large scatter for both models, while the distances from other methods mostly stay on the line of unity. There are systematic discrepancies in the distributions of distances and inclinations for both models: Einasto prefers smaller distances and inclinations, while DC14 prefer larger values.

Interestingly, Einasto and DC14 show opposite systematics. Smaller  $D$  corresponds to a smaller contribution of baryonic matter, while smaller inclinations lead to an increase in the amplitude of rotation velocities. This suggests that Einasto haloes provide a systematically larger contribution to the total rotation velocities than DC14 haloes.

## A2 Priors of halo parameters

To check whether the  $\Lambda$ CDM priors we impose are recovered, we plot the SHM and mass-concentration relations for both models in Figure A3. Both models show tight SHM relations. Most galaxies are well within the  $2\sigma$  region of the fiducial abundance-matching scatter. The Einasto model gives a slightly tighter SHM relation than does DC14. However, the resultant mass-concentration relations show large discrepancies for both models. There are 26.3% and 30.3% of the total galaxies outside  $2\sigma$  regions for Einasto and DC14 profiles, respectively. The fractions are larger than the expectation of the  $2\sigma$  confidence region (5%). Again, Einasto and DC14

## Einasto

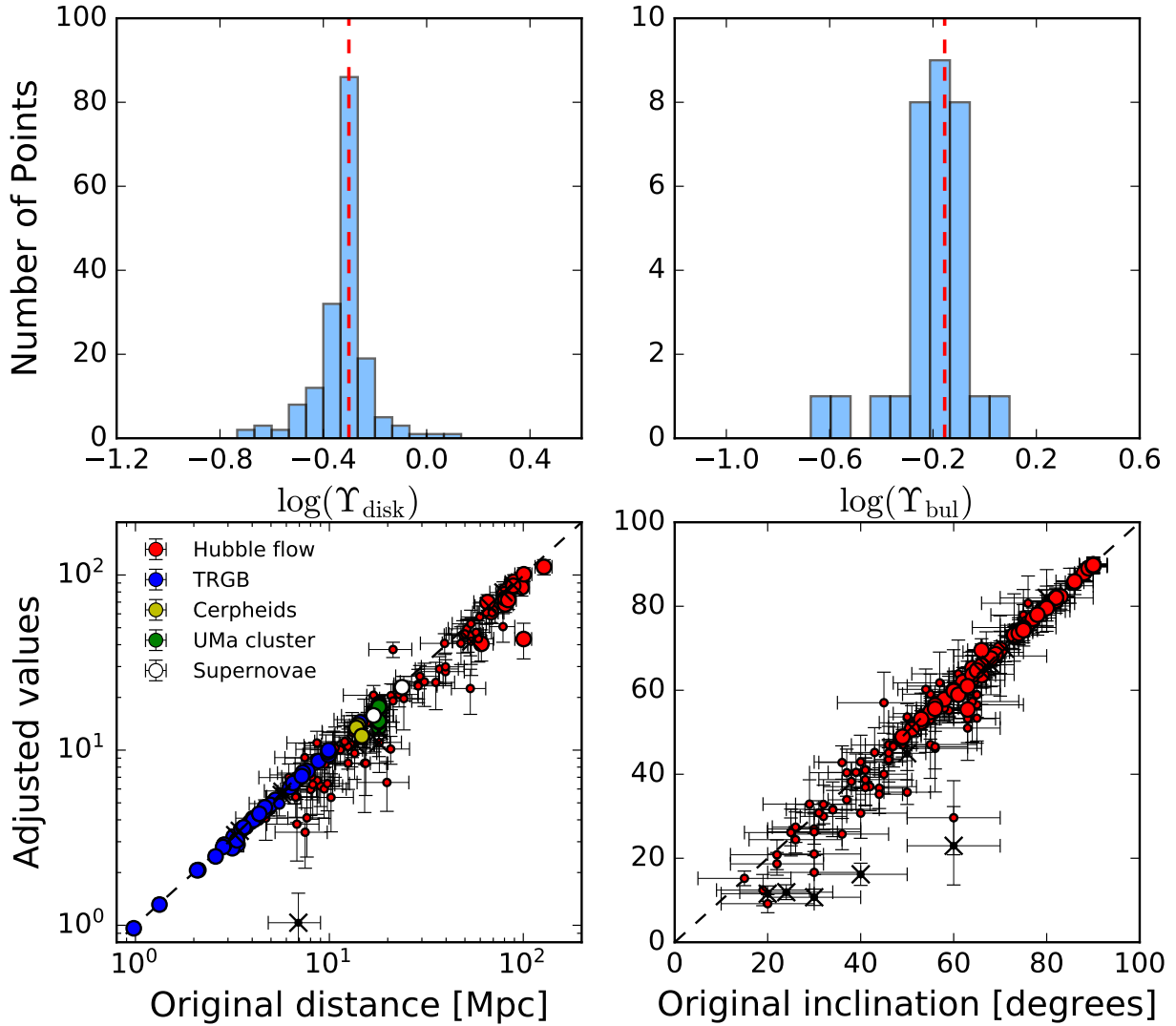


**Figure A1.** Distributions of optimized galactic parameters for Einasto model. Top panels show the histograms of stellar mass-to-light ratio for discs (top-left) and bulges (top-right). Red dashed lines indicate their fiducial values according to [Lelli et al. \(2016\)](#). In the bottom panels, we plot the optimized galaxy distances and disc inclinations against their original values. Different methods of measuring galaxy distances are represented by different colors. Large and small points represent galaxies with observational errors larger and smaller than 15% for distances and 5% for inclinations, respectively. Galaxies with low-quality flag ( $Q=3$ , see [Lelli et al. 2016](#)) are marked as black crosses. Black dashed lines are line of unity.

show opposite systematics: smaller and larger concentrations are preferred for Einasto and DC14 models, respectively. Recalling that the Einasto profile requires smaller contributions from baryonic distributions and larger observational rotational velocities compared to the DC14 profile, it seems contradictory that it still prefers smaller concentrations than DC14.

This effect is due to the exponential decrease of halo density in Einasto model at large radii. If the shape parameter  $\alpha_\epsilon > 0.2$ , the density decrease of Einasto halo is faster than an NFW profile (see Figure 2 in [Dutton & Mac-](#)

[ciò 2014](#)). For the same total halo mass ( $M_{\text{halo}}$ ), Einasto model with  $\alpha_\epsilon > 0.2$  places more mass closer to the center. Although this may make outer DM distribution insufficient to support a flat rotation curve, it would not contradict the data since rotation curves are not available at large radii. Therefore, when fitting rotation curves, MCMC enlarges the total rotation velocities by decreasing inclination. In the meantime, decreasing concentration could also decrease the inner mass and hence reduce halo contributions. To check this, we use blue colour to mark those galaxies with  $\alpha_\epsilon > 0.3$  (instead of 0.2 for better illustration) in Figure A3.

## DC14

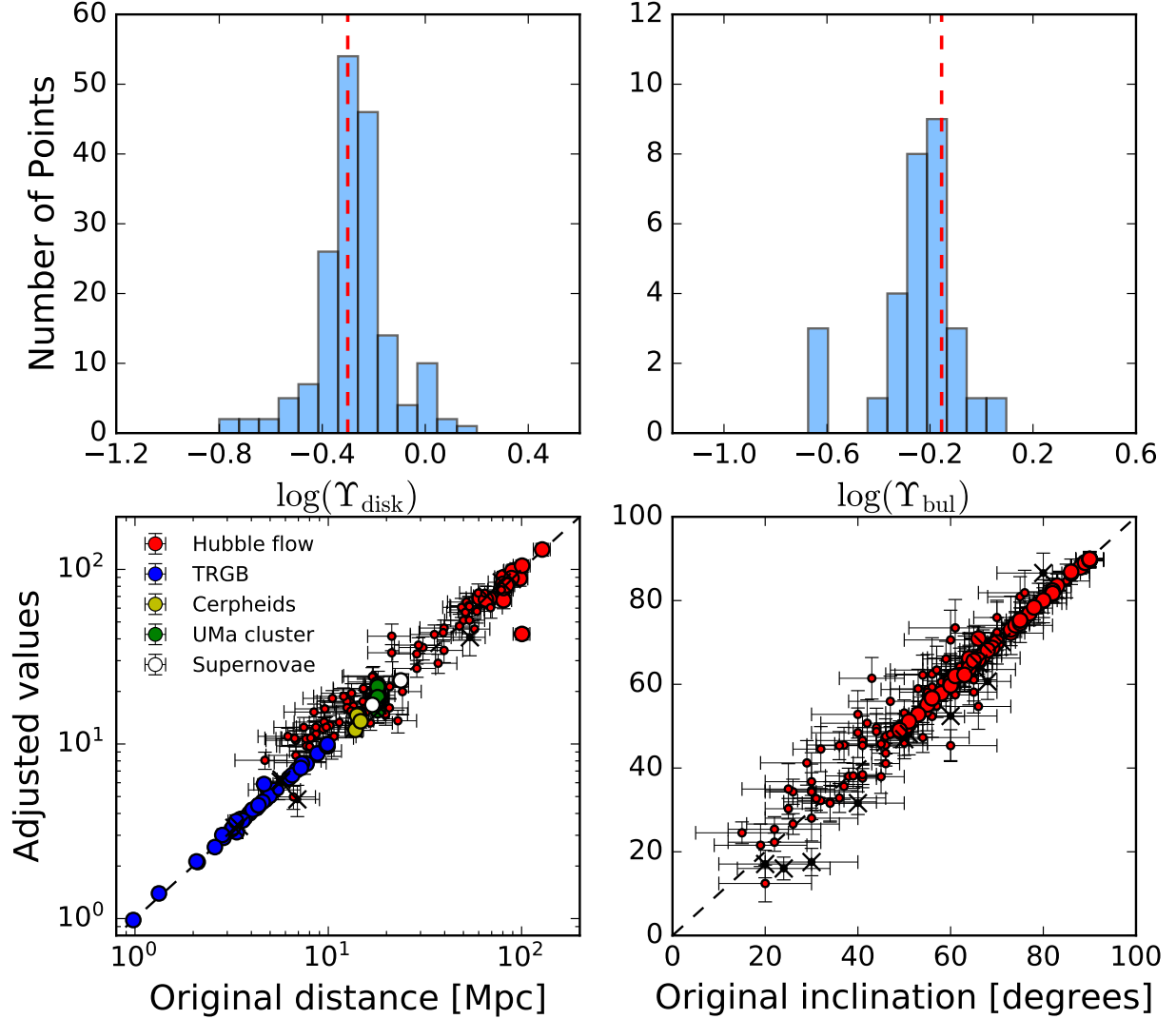


**Figure A2.** Same as Figure A1 but for DC14 model.

Consequently, blue points apparently represent those galaxies with smaller concentration than expected.

In Figure A4, we plot the values of  $\alpha_\epsilon$  against galaxy luminosity and halo mass for both  $\Lambda$ CDM priors (left) and flat priors (right). In the case of  $\Lambda$ CDM priors,  $\alpha_\epsilon$  is constant with galaxy luminosity but larger than expected for galaxies with halo mass smaller than  $10^{11.5} M_\odot$ . These galaxies are typically dwarf galaxies with slowly-rising rotation curves. Large values of  $\alpha_\epsilon$  reduce the central density and give better fits to the rotation curves. In the case of flat priors, the distribution of  $\alpha_\epsilon$  shows a significantly larger scatter. Most galaxies have a value of  $\alpha_\epsilon$  larger than 0.3. This is qualitatively consistent with the finding in Chemin et al. (2011) while in clear contrast to  $\Lambda$ CDM simulations. Navarro et al. (2004, 2010) show that the simulated DM haloes for dwarf galaxies, large spirals and clusters are consistently better

fit by the Einasto profile with  $\alpha_\epsilon$  in the range of [0.1, 0.2]. Tissera et al. (2010) add baryons into their simulation and consider the feedbacks in galaxy formation. The resultant values of  $\alpha_\epsilon$  remain in the same range. Thus, although the simulation-motivated Einasto profile can well describe the rotation curves of late-type galaxies, the shape parameter presents a considerable discrepancy from what simulations predict.

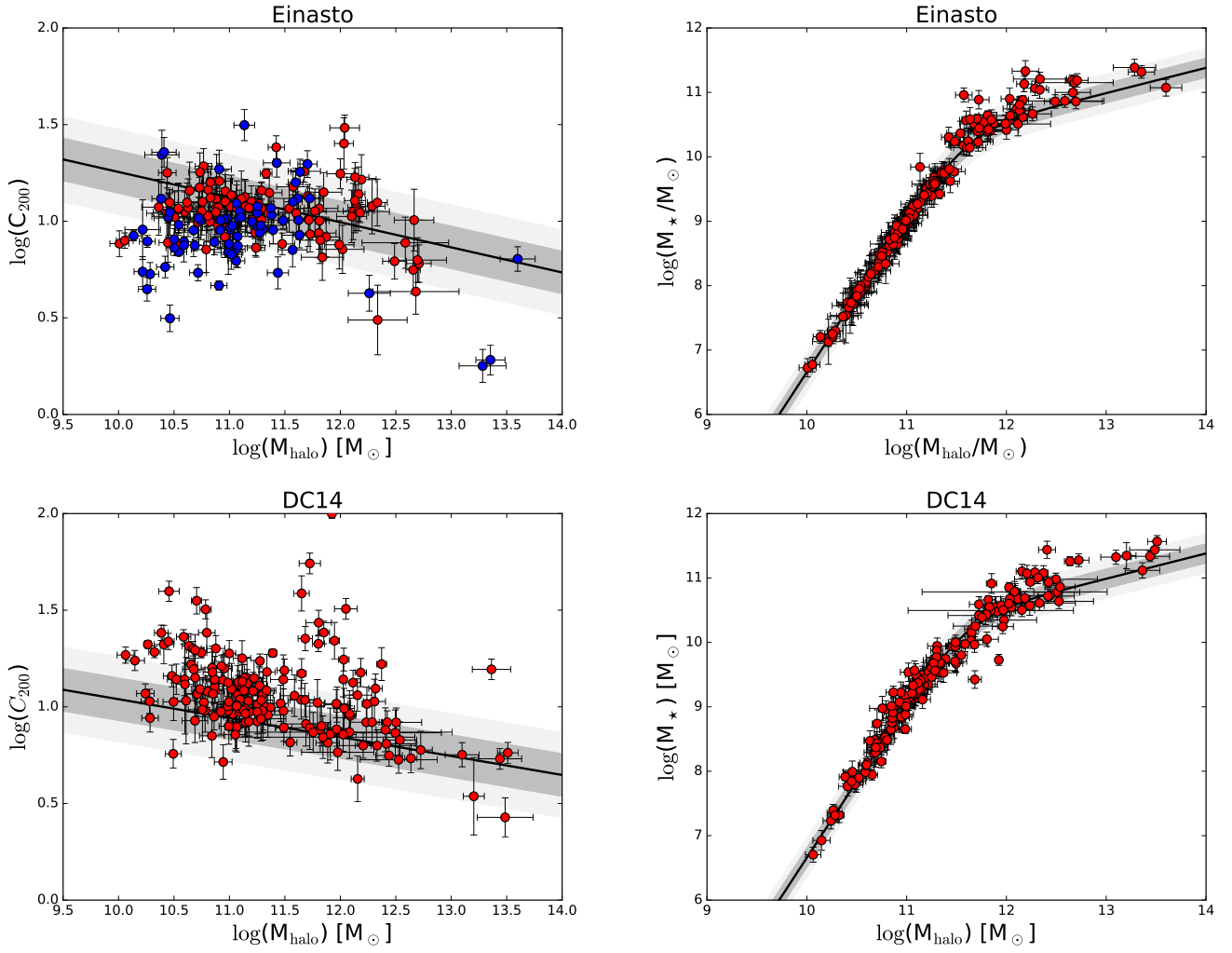


**Figure A3.** Halo mass-concentration relation (left) and stellar mass-halo mass relation (right) for Einasto (top) and DC14 (bottom) when  $\Lambda$ CDM priors are imposed. Solid lines show the expected mean relation from cosmological simulations; dark and light bands show  $1\sigma$  and  $2\sigma$  confidence regions, respectively. Blue points represent galaxies with  $\alpha_{\epsilon} > 0.3$  in the Einasto profile. This is the manifestation of the cusp-core problem, as these galaxies violate the  $\Lambda$ CDM expectation for  $\alpha_{\epsilon}$  even if they fall within the range expected for the mass-concentration relation.

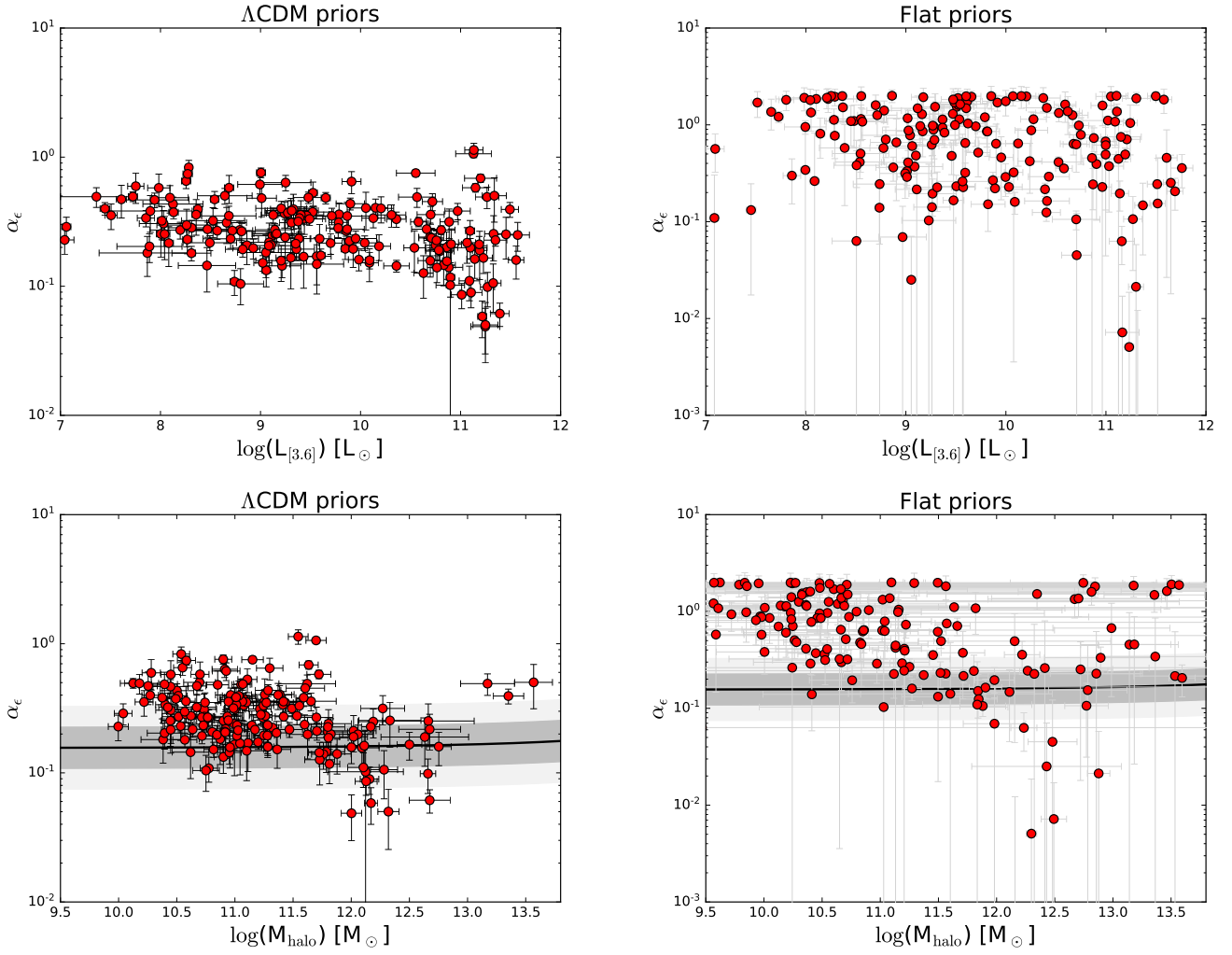


**Figure A4.** The shape parameter  $\alpha_\epsilon$  of the Einasto model versus  $L_{[3.6]}$  (top panels) and  $M_{\text{halo}}$  (bottom panels), when imposing  $\Lambda$ CDM priors (left) and flat priors (right). The solid line in the bottom panels is the median relation expected from cosmological simulations and the dark and light regions correspond to  $1\sigma$  and  $2\sigma$  standard deviations, respectively. The cusp-core problem manifests itself by driving  $\alpha_\epsilon$  to larger values than expected in  $\Lambda$ CDM. Note that this problem sometimes occurs at high as well as low mass.



**Table A1.** The best-fit values of halo parameters and fit goodness for the Einasto profile with both  $\Lambda$ CDM priors (middle panel) and flat priors (right panel). Some galaxies have more fitting parameters than the data points in their observed rotation curves, so their  $\chi^2_\nu$  are blank.

SPARC ID	Galaxy Name	$\alpha_\epsilon$	$r_s$ kpc	$\log \rho_s$ [ $M_\odot \text{pc}^{-3}$ ]	$\chi^2_\nu$	$\alpha_\epsilon$	$r_s$ kpc	$\log \rho_s$ [ $M_\odot \text{pc}^{-3}$ ]	$\chi^2_\nu$
001	UGC02487	0.25 ± 0.06	12.84 ± 3.70	-2.03 ± 0.41	6.427	0.36 ± 0.13	26.66 ± 10.42	-2.76 ± 0.54	5.769
002	UGC02885	0.16 ± 0.05	65.25 ± 16.89	-3.43 ± 0.36	1.095	0.25 ± 0.23	79.61 ± 35.25	-3.61 ± 0.66	1.036
003	NGC6195	0.25 ± 0.09	78.15 ± 31.84	-3.64 ± 0.67	2.169	1.82 ± 0.51	24.04 ± 23.32	-2.78 ± 1.76	1.844
004	UGC11455	0.69 ± 0.05	8.49 ± 1.39	-1.64 ± 0.23	2.040	0.75 ± 0.06	7.99 ± 1.67	-1.59 ± 0.29	2.076
005	NGC5371	0.05 ± 0.02	7.15 ± 2.03	-1.97 ± 0.43	2.459	0.00 ± 0.01	16.05 ± 28.16	-3 ± 185191	1.629
006	NGC2955	0.06 ± 0.01	35.26 ± 14.55	-2.98 ± 0.59	2.874	1.98 ± 0.19	14.06 ± 1.85	-2.13 ± 0.20	2.857
007	NGC0801	0.25 ± 0.10	83.35 ± 38.28	-3.94 ± 0.67	8.062	0.15 ± 0.30	701 ± 1516	-5.41 ± 3.11	7.686
008	ESO563-G021	1.06 ± 0.06	8.00 ± 1.37	-1.36 ± 0.24	9.000	1.11 ± 0.06	7.02 ± 2.18	-1.24 ± 0.43	9.037
009	UGC09133	0.05 ± 0.02	19.44 ± 5.32	-2.69 ± 0.46	7.042	0.01 ± 0.01	3.04 ± 0.85	-1.00 ± 0.40	6.444
010	UGC02953	0.23 ± 0.02	20.67 ± 2.73	-2.64 ± 0.19	5.712	0.24 ± 0.03	25.22 ± 3.22	-2.76 ± 0.18	5.701
011	NGC7331	0.17 ± 0.04	48.50 ± 11.20	-3.33 ± 0.33	0.746	0.11 ± 0.07	136.3 ± 121.0	-4.12 ± 1.23	0.736
012	NGC3992	0.11 ± 0.04	20.82 ± 7.12	-2.71 ± 0.47	1.378	0.15 ± 0.10	13.69 ± 16.19	-2.34 ± 1.59	0.913
013	NGC6674	0.49 ± 0.09	266.24 ± 69.08	-4.37 ± 0.42	1.781	0.46 ± 0.43	473.3 ± 407.2	-4.82 ± 1.27	1.618
014	NGC5985	0.20 ± 0.04	7.00 ± 1.29	-1.51 ± 0.28	2.423	0.22 ± 0.03	2.98 ± 0.89	-0.73 ± 0.45	2.133
015	NGC2841	0.10 ± 0.03	59.30 ± 17.15	-3.45 ± 0.40	1.470	0.02 ± 0.04	3297 ± 55365	-6.76 ± 23.36	1.367
016	IC4202	0.75 ± 0.04	3.41 ± 0.69	-0.90 ± 0.28	7.304	0.78 ± 0.04	0.59 ± 0.11	0.65 ± 0.27	5.993
017	NGC5005	0.19 ± 0.08	45.49 ± 19.92	-3.14 ± 0.69	0.100	1.05 ± 0.56	8.63 ± 15.19	-2.00 ± 3.22	0.118
018	NGC5907	0.06 ± 0.02	16.82 ± 5.58	-2.65 ± 0.46	4.133	0.01 ± 0.01	116 ± 1393	-4.33 ± 16.51	3.527
019	UGC05253	0.58 ± 0.04	12.36 ± 1.78	-2.10 ± 0.22	0.775	0.71 ± 0.15	13.99 ± 2.44	-2.25 ± 0.26	0.769
020	NGC5055	0.21 ± 0.03	11.81 ± 1.71	-2.43 ± 0.20	2.846	0.49 ± 0.08	17.28 ± 1.85	-2.78 ± 0.16	2.748
021	NGC2998	0.09 ± 0.02	19.77 ± 5.69	-2.77 ± 0.40	1.201	0.06 ± 0.03	30.11 ± 22.94	-3.14 ± 1.04	1.103
022	UGC11914	0.50 ± 0.19	99.77 ± 18.59	-3.01 ± 0.31	0.747	1.88 ± 0.28	74.65 ± 14.65	-2.25 ± 0.34	0.527
023	NGC3953	0.11 ± 0.03	21.86 ± 7.63	-2.88 ± 0.49	1.571	0.45 ± 0.56	5.59 ± 9.57	-1.76 ± 2.88	0.563
024	UGC12506	0.16 ± 0.05	12.93 ± 2.61	-2.25 ± 0.30	0.211	0.20 ± 0.07	10.59 ± 2.65	-2.08 ± 0.39	0.167
025	NGC0891	0.27 ± 0.05	9.03 ± 1.55	-2.03 ± 0.28	4.047	1.37 ± 0.27	7.22 ± 0.62	-1.77 ± 0.13	1.280
026	UGC06614	0.22 ± 0.07	53.38 ± 17.87	-3.26 ± 0.52	0.432	1.08 ± 0.50	30.84 ± 20.53	-2.99 ± 1.17	0.099
027	UGC02916	1.14 ± 0.14	11.29 ± 1.18	-1.94 ± 0.16	9.816	2.00 ± 0.11	9.41 ± 1.19	-2.01 ± 0.19	9.183
028	UGC03205	0.09 ± 0.02	16.85 ± 6.41	-2.64 ± 0.52	3.091	0.11 ± 0.02	4.73 ± 2.46	-1.47 ± 0.72	2.934
029	NGC5033	0.38 ± 0.06	9.22 ± 1.66	-2.02 ± 0.25	2.507	0.62 ± 0.11	11.41 ± 2.07	-2.20 ± 0.26	2.220
030	NGC4088	0.20 ± 0.06	22.29 ± 6.97	-3.04 ± 0.45	0.789	0.67 ± 0.54	111.66 ± 57.94	-3.61 ± 0.86	0.728
031	NGC4157	0.21 ± 0.07	29.42 ± 9.75	-3.16 ± 0.48	0.670	0.49 ± 0.45	44.99 ± 33.04	-3.36 ± 1.28	0.457
032	UGC03546	0.19 ± 0.04	11.52 ± 2.94	-2.35 ± 0.38	1.102	0.73 ± 0.20	9.27 ± 1.54	-2.15 ± 0.27	0.747
033	UGC06787	0.39 ± 0.05	300.91 ± 62.55	-4.37 ± 0.31	18.308	0.21 ± 0.07	1756 ± 2083	-5.57 ± 1.74	17.897
034	NGC4051	0.15 ± 0.04	18.50 ± 5.62	-2.93 ± 0.43	4.150	1.58 ± 0.61	4.60 ± 11.92	-1.86 ± 4.20	1.499
035	NGC4217	0.36 ± 0.06	12.15 ± 3.36	-2.33 ± 0.42	3.191	1.50 ± 0.29	3.81 ± 1.07	-1.28 ± 0.39	1.373
036	NGC3521	0.10 ± 0.11	20.51 ± 8.81	-2.82 ± 0.67	0.324	1.96 ± 0.52	15.41 ± 21.55	-2.46 ± 2.56	0.179
037	NGC2903	0.27 ± 0.02	5.46 ± 0.83	-1.66 ± 0.21	6.308	0.29 ± 0.03	3.35 ± 0.64	-1.23 ± 0.28	6.191
038	NGC2683	0.12 ± 0.03	16.79 ± 5.64	-2.84 ± 0.46	3.066	0.39 ± 0.29	6.85 ± 3.93	-2.00 ± 0.85	1.705
039	NGC4013	0.32 ± 0.08	58.90 ± 15.32	-3.63 ± 0.39	0.918	0.23 ± 0.39	223.5 ± 206.9	-4.47 ± 1.34	0.830
040	NGC7814	0.16 ± 0.04	16.84 ± 4.05	-2.57 ± 0.35	0.604	0.24 ± 0.11	11.17 ± 4.29	-2.23 ± 0.63	0.593
041	UGC06786	0.19 ± 0.03	11.57 ± 2.32	-2.16 ± 0.29	0.665	0.16 ± 0.04	6.49 ± 1.61	-1.64 ± 0.36	0.542
042	NGC3877	0.24 ± 0.04	10.11 ± 2.32	-2.31 ± 0.34	6.521	1.26 ± 0.31	3.49 ± 0.59	-1.37 ± 0.25	2.685
043	NGC0289	0.14 ± 0.04	21.65 ± 5.42	-3.02 ± 0.35	2.205	0.37 ± 0.25	31.51 ± 17.31	-3.40 ± 0.76	2.033
044	NGC1090	0.28 ± 0.04	12.10 ± 3.68	-2.53 ± 0.42	2.419	0.41 ± 0.05	6.83 ± 2.43	-1.98 ± 0.49	1.808
045	NGC3726	0.24 ± 0.07	24.53 ± 7.25	-3.12 ± 0.44	3.939	0.45 ± 0.52	206.3 ± 112.7	-4.17 ± 0.85	2.871
046	UGC09037	0.45 ± 0.07	17.33 ± 3.41	-2.74 ± 0.31	1.327	0.99 ± 0.33	12.07 ± 2.42	-2.46 ± 0.34	1.143
047	NGC6946	0.23 ± 0.04	21.02 ± 5.24	-2.97 ± 0.36	1.753	0.63 ± 0.31	8.70 ± 2.34	-2.30 ± 0.45	1.566
048	NGC4100	0.14 ± 0.03	14.41 ± 3.86	-2.69 ± 0.37	1.370	0.64 ± 0.15	5.21 ± 0.99	-1.65 ± 0.29	0.419
049	NGC3893	0.21 ± 0.05	14.33 ± 4.10	-2.57 ± 0.42	1.614	0.79 ± 0.40	7.13 ± 3.03	-1.96 ± 0.70	0.522
050	UGC06973	0.36 ± 0.07	6.37 ± 1.23	-1.74 ± 0.29	2.494	0.88 ± 0.48	3.30 ± 5.31	-1.23 ± 2.94	2.568
051	ESO079-G014	0.49 ± 0.08	14.86 ± 4.43	-2.50 ± 0.46	2.861	1.33 ± 0.25	8.09 ± 2.15	-1.99 ± 0.37	0.962
052	UGC08699	0.16 ± 0.04	26.35 ± 7.97	-3.11 ± 0.42	0.787	0.05 ± 0.08	707 ± 5541	-5.70 ± 10.94	0.691
053	NGC4138	0.13 ± 0.05	15.07 ± 4.85	-2.78 ± 0.45		1.38 ± 0.58	4.54 ± 5.78	-1.58 ± 1.78	
054	NGC3198	0.31 ± 0.03	13.74 ± 1.45	-2.68 ± 0.15	1.119	0.35 ± 0.03	13.87 ± 1.54	-2.68 ± 0.16	1.081
055	NGC3949	0.20 ± 0.07	14.47 ± 4.26	-2.74 ± 0.42	2.160	1.62 ± 0.56	73.91 ± 38.44	-2.37 ± 0.79	1.615
056	NGC6015	0.14 ± 0.01	15.96 ± 3.97	-2.82 ± 0.34	7.830	0.12 ± 0.02	24.39 ± 12.56	-3.18 ± 0.71	7.821
057	NGC3917	0.33 ± 0.04	19.89 ± 4.52	-3.04 ± 0.33	3.331	1.14 ± 0.21	6.12 ± 0.92	-2.00 ± 0.22	1.413
058	NGC4085	0.40 ± 0.09	10.70 ± 2.09	-2.40 ± 0.29	15.519	1.98 ± 0.50	3.23 ± 11.62	-1.48 ± 6.63	7.827
059	NGC4389	0.40 ± 0.13	12.07 ± 2.91	-2.66 ± 0.35		1.98 ± 0.41	32.55 ± 17.10	-1.98 ± 0.93	
060	NGC4559	0.23 ± 0.03	9.54 ± 2.92	-2.53 ± 0.42	0.253	1.89 ± 0.53	12.55 ± 4.61	-2.78 ± 0.56	0.105

**Table A1** – *continued*

SPARC ID	Galaxy Name	$\alpha_\epsilon$	$r_s$ kpc	$\log \rho_s$ [ $M_\odot \text{pc}^{-3}$ ]	$\chi^2_\nu$	$\alpha_\epsilon$	$r_s$ kpc	$\log \rho_s$ [ $M_\odot \text{pc}^{-3}$ ]	$\chi^2_\nu$
061	NGC3769	0.20 ± 0.05	11.68 ± 2.74	-2.72 ± 0.32	1.178	0.42 ± 0.23	10.78 ± 3.38	-2.62 ± 0.50	0.985
062	NGC4010	0.41 ± 0.07	14.08 ± 2.67	-2.73 ± 0.28	2.958	1.97 ± 0.46	6.27 ± 3.73	-2.10 ± 1.07	1.613
063	NGC3972	0.34 ± 0.05	12.42 ± 2.40	-2.61 ± 0.28	1.541	0.64 ± 0.27	6.74 ± 8.71	-2.14 ± 2.35	1.243
064	UGC03580	0.33 ± 0.04	9.49 ± 1.53	-2.44 ± 0.23	2.349	0.23 ± 0.07	12.74 ± 3.28	-2.65 ± 0.39	2.347
065	NGC6503	0.16 ± 0.02	8.01 ± 0.88	-2.43 ± 0.15	1.426	0.16 ± 0.04	7.68 ± 0.99	-2.39 ± 0.20	1.411
066	UGC11557	0.35 ± 0.10	11.40 ± 3.81	-2.62 ± 0.50	1.483	1.75 ± 0.51	5.64 ± 16.34	-1.98 ± 5.28	0.605
067	UGC00128	0.22 ± 0.03	17.77 ± 2.79	-3.07 ± 0.24	3.855	0.23 ± 0.03	16.90 ± 3.20	-2.93 ± 0.28	3.796
068	F579-V1	0.15 ± 0.04	8.79 ± 2.62	-2.48 ± 0.41	0.489	0.32 ± 0.32	3.72 ± 3.09	-1.85 ± 1.50	0.217
069	NGC4183	0.16 ± 0.03	11.61 ± 2.46	-2.83 ± 0.29	0.293	0.29 ± 0.11	7.50 ± 2.65	-2.46 ± 0.56	0.193
070	F571-8	0.63 ± 0.09	4.68 ± 1.13	-1.61 ± 0.34	0.998	1.30 ± 0.32	4.54 ± 1.22	-1.58 ± 0.39	0.608
071	NGC2403	0.22 ± 0.01	6.77 ± 0.48	-2.10 ± 0.11	9.178	0.22 ± 0.01	6.86 ± 0.52	-2.07 ± 0.11	9.086
072	UGC06930	0.19 ± 0.05	11.10 ± 2.84	-2.74 ± 0.36	0.631	0.46 ± 0.29	7.23 ± 3.96	-2.37 ± 0.94	0.352
073	F568-3	0.65 ± 0.13	13.02 ± 2.87	-2.55 ± 0.32	1.873	1.70 ± 0.31	7.30 ± 3.00	-2.21 ± 0.67	1.231
074	UGC01230	0.28 ± 0.09	9.45 ± 2.28	-2.48 ± 0.35	1.626	0.64 ± 0.38	7.85 ± 6.86	-2.34 ± 1.41	0.738
075	NGC0247	0.27 ± 0.02	15.38 ± 1.97	-3.07 ± 0.19	1.775	0.27 ± 0.06	16.01 ± 5.00	-3.10 ± 0.49	1.775
076	NGC7793	0.20 ± 0.03	12.73 ± 3.56	-2.92 ± 0.38	0.967	1.98 ± 0.52	3.91 ± 1.99	-2.12 ± 0.90	0.654
077	UGC06917	0.28 ± 0.04	11.18 ± 2.05	-2.71 ± 0.26	1.113	0.85 ± 0.38	5.43 ± 3.16	-2.13 ± 1.05	0.455
078	NGC1003	0.35 ± 0.05	23.58 ± 4.74	-3.32 ± 0.28	2.579	0.15 ± 0.07	78.23 ± 45.59	-4.25 ± 0.81	2.478
079	F574-1	0.31 ± 0.05	10.92 ± 2.13	-2.66 ± 0.28	1.353	0.86 ± 0.26	5.54 ± 1.12	-2.19 ± 0.35	0.229
080	F568-1	0.36 ± 0.08	10.28 ± 2.08	-2.50 ± 0.29	0.810	1.20 ± 0.47	5.25 ± 3.95	-1.84 ± 1.36	0.178
081	UGC06983	0.22 ± 0.04	8.91 ± 1.65	-2.56 ± 0.26	0.853	0.52 ± 0.23	5.86 ± 2.08	-2.19 ± 0.63	0.597
082	UGC05986	0.44 ± 0.05	13.79 ± 2.72	-2.77 ± 0.28	3.504	1.49 ± 0.23	3.81 ± 1.14	-1.67 ± 0.41	0.089
083	NGC0055	0.48 ± 0.05	15.52 ± 1.48	-3.10 ± 0.15	1.221	1.95 ± 0.27	7.33 ± 0.66	-2.54 ± 0.15	0.164
084	ESO116-G012	0.38 ± 0.04	8.22 ± 2.01	-2.38 ± 0.34	1.774	0.97 ± 0.37	5.94 ± 1.76	-2.15 ± 0.44	0.975
085	UGC07323	0.38 ± 0.08	9.42 ± 2.86	-2.60 ± 0.43	0.961	0.26 ± 0.54	83.67 ± 82.75	-3.89 ± 1.60	0.453
086	UGC05005	0.36 ± 0.10	12.69 ± 3.44	-2.93 ± 0.39	0.957	1.03 ± 0.50	15.00 ± 20.27	-2.98 ± 2.42	0.016
087	F561-1	0.17 ± 0.07	8.52 ± 2.70	-2.62 ± 0.44		1.75 ± 0.59	3.77 ± 21.01	-2.56 ± 9.61	
088	NGC0024	0.17 ± 0.02	8.34 ± 1.61	-2.53 ± 0.27	0.868	0.32 ± 0.08	3.83 ± 1.09	-1.83 ± 0.48	0.838
089	F568-V1	0.23 ± 0.07	8.15 ± 1.88	-2.46 ± 0.32	0.323	0.65 ± 0.35	5.14 ± 3.70	-1.98 ± 1.28	0.117
090	UGC06628	0.15 ± 0.06	7.86 ± 2.85	-2.58 ± 0.51	0.484	1.63 ± 0.59	1.79 ± 9.06	-1.91 ± 8.90	0.067
091	UGC02455	0.38 ± 0.12	2.61 ± 0.82	-1.59 ± 0.46	6.289	1.85 ± 0.44	21.35 ± 11.54	-1.01 ± 0.85	1.523
092	UGC07089	0.34 ± 0.08	14.11 ± 2.71	-3.12 ± 0.27	0.400	0.23 ± 0.51	162.0 ± 210.5	-4.54 ± 2.00	0.160
093	UGC05999	0.40 ± 0.12	10.98 ± 2.83	-2.76 ± 0.38		1.70 ± 0.49	8.50 ± 8.20	-2.35 ± 1.67	
094	NGC2976	0.53 ± 0.11	9.66 ± 1.77	-2.43 ± 0.26	0.519	1.89 ± 0.48	2.32 ± 12.26	-1.50 ± 9.73	0.337
095	UGC05750	0.37 ± 0.09	13.51 ± 3.78	-3.06 ± 0.39	0.973	1.61 ± 0.49	9.52 ± 5.90	-2.77 ± 1.09	0.088
096	NGC0100	0.40 ± 0.05	8.84 ± 2.52	-2.55 ± 0.40	0.372	1.14 ± 0.43	6.41 ± 6.61	-2.38 ± 1.85	0.130
097	UGC00634	0.39 ± 0.09	11.22 ± 3.18	-2.78 ± 0.40		1.00 ± 0.37	10.35 ± 3.93	-2.62 ± 0.59	
098	F563-V2	0.33 ± 0.08	8.76 ± 2.38	-2.50 ± 0.38	1.446	1.54 ± 0.46	3.76 ± 3.52	-1.64 ± 1.58	0.140
099	NGC5585	0.49 ± 0.05	13.52 ± 1.95	-2.92 ± 0.21	6.758	1.98 ± 0.15	6.80 ± 0.99	-2.41 ± 0.20	4.247
100	NGC0300	0.35 ± 0.05	10.22 ± 2.09	-2.65 ± 0.28	0.533	0.48 ± 0.17	7.78 ± 3.69	-2.46 ± 0.80	0.502
101	UGC06923	0.23 ± 0.07	10.27 ± 2.18	-2.84 ± 0.30		1.83 ± 0.54	3.57 ± 16.68	-2.01 ± 8.61	
102	F574-2	0.17 ± 0.07	8.59 ± 2.99	-2.69 ± 0.47		0.17 ± 0.52	13.5 ± 201.6	-4.88 ± 27.28	
103	UGC07125	0.22 ± 0.03	6.07 ± 2.19	-2.59 ± 0.49	0.730	0.70 ± 0.38	6.46 ± 2.20	-2.78 ± 0.53	0.282
104	UGC07524	0.32 ± 0.04	12.10 ± 1.54	-2.98 ± 0.19	0.495	0.83 ± 0.25	5.55 ± 1.10	-2.42 ± 0.36	0.210
105	UGC06399	0.31 ± 0.06	9.89 ± 1.66	-2.74 ± 0.24	1.149	1.14 ± 0.49	4.64 ± 5.71	-2.13 ± 2.25	0.096
106	UGC07151	0.21 ± 0.03	12.73 ± 2.11	-3.08 ± 0.23	4.428	0.94 ± 0.31	2.47 ± 0.73	-1.84 ± 0.53	2.034
107	F567-2	0.17 ± 0.07	7.26 ± 2.32	-2.55 ± 0.44		1.54 ± 0.56	3.18 ± 11.85	-2.38 ± 6.37	
108	UGC04325	0.19 ± 0.03	6.94 ± 1.76	-2.45 ± 0.35	9.354	0.89 ± 0.23	2.10 ± 0.59	-1.40 ± 0.41	1.414
109	UGC00191	0.25 ± 0.03	6.85 ± 1.86	-2.45 ± 0.38	6.496	0.37 ± 0.06	4.15 ± 1.35	-2.13 ± 0.49	5.146
110	F563-1	0.37 ± 0.08	9.31 ± 2.22	-2.62 ± 0.34	1.148	0.62 ± 0.25	7.56 ± 3.51	-2.31 ± 0.78	0.929
111	F571-V1	0.24 ± 0.09	9.89 ± 2.70	-2.81 ± 0.38	4.005	0.95 ± 0.51	8.27 ± 12.99	-2.65 ± 2.82	0.192
112	UGC07261	0.16 ± 0.05	7.04 ± 2.36	-2.56 ± 0.47	0.094	0.10 ± 0.29	16.25 ± 30.25	-3.40 ± 2.72	0.122
113	UGC10310	0.21 ± 0.05	7.88 ± 2.47	-2.66 ± 0.44	3.113	0.98 ± 0.50	3.27 ± 3.21	-2.07 ± 1.73	0.420
114	UGC02259	0.14 ± 0.03	6.03 ± 1.51	-2.42 ± 0.35	2.099	0.19 ± 0.08	4.52 ± 2.22	-2.18 ± 0.75	1.987
115	F583-4	0.25 ± 0.05	9.55 ± 2.69	-2.83 ± 0.39	0.334	0.14 ± 0.34	88.1 ± 199.2	-4.51 ± 3.23	0.222
116	UGC12732	0.26 ± 0.04	11.04 ± 3.00	-2.96 ± 0.38	0.304	0.23 ± 0.10	16.70 ± 8.66	-3.29 ± 0.81	0.215
117	UGC06818	0.48 ± 0.14	10.60 ± 1.78	-2.83 ± 0.26	6.691	1.93 ± 0.47	9.34 ± 25.83	-2.54 ± 5.09	3.241
118	UGC04499	0.27 ± 0.04	6.91 ± 2.07	-2.56 ± 0.41	1.793	0.86 ± 0.39	4.38 ± 2.75	-2.29 ± 1.07	0.615
119	F563-V1	0.18 ± 0.07	8.57 ± 3.10	-2.81 ± 0.51		1.29 ± 0.57	2.63 ± 39.04	-2.97 ± 27.24	
120	UGC06667	0.36 ± 0.05	9.07 ± 1.28	-2.64 ± 0.21	1.527	0.97 ± 0.34	4.38 ± 1.59	-2.07 ± 0.65	0.150

**Table A1** – *continued*

SPARC ID	Galaxy Name	$\alpha_\epsilon$	$r_s$ kpc	$\log \rho_s$ [ $M_\odot \text{pc}^{-3}$ ]	$\chi^2_\nu$	$\alpha_\epsilon$	$r_s$ kpc	$\log \rho_s$ [ $M_\odot \text{pc}^{-3}$ ]	$\chi^2_\nu$
121	UGC02023	0.22 ± 0.09	7.71 ± 2.81	-2.62 ± 0.51		1.48 ± 0.50	73.94 ± 73.18	-2.51 ± 1.36	
122	UGC04278	0.61 ± 0.10	9.75 ± 2.28	-2.57 ± 0.33	0.821	0.22 ± 0.40	420.6 ± 563.8	-4.56 ± 1.89	0.571
123	UGC12632	0.23 ± 0.04	6.39 ± 1.84	-2.55 ± 0.40	0.414	0.60 ± 0.27	4.68 ± 1.80	-2.35 ± 0.64	0.111
124	UGC08286	0.21 ± 0.02	7.52 ± 1.07	-2.61 ± 0.21	3.118	0.48 ± 0.08	3.41 ± 0.34	-1.94 ± 0.18	1.885
125	UGC07399	0.27 ± 0.03	5.64 ± 1.33	-2.16 ± 0.33	1.448	0.41 ± 0.14	3.36 ± 1.53	-1.72 ± 0.75	1.000
126	NGC4214	0.13 ± 0.03	5.40 ± 1.77	-2.37 ± 0.44	0.755	0.03 ± 0.05	233 ± 5286	-4.83 ± 31.34	0.179
127	UGC05414	0.35 ± 0.07	7.58 ± 2.62	-2.62 ± 0.47		0.87 ± 0.53	4.47 ± 20.39	-2.38 ± 8.39	
128	UGC08490	0.15 ± 0.02	4.99 ± 0.97	-2.32 ± 0.27	0.352	0.29 ± 0.07	3.09 ± 0.63	-1.91 ± 0.33	0.116
129	IC2574	0.76 ± 0.06	18.49 ± 1.46	-3.34 ± 0.13	2.395	0.33 ± 0.10	247.1 ± 159.1	-4.51 ± 1.00	2.058
130	UGC06446	0.20 ± 0.03	6.47 ± 1.69	-2.51 ± 0.36	0.311	0.32 ± 0.14	4.45 ± 2.14	-2.21 ± 0.79	0.254
131	F583-1	0.50 ± 0.07	6.95 ± 1.79	-2.43 ± 0.37	0.626	1.17 ± 0.28	6.59 ± 1.66	-2.42 ± 0.36	0.182
132	UGC11820	0.27 ± 0.04	10.88 ± 3.18	-3.09 ± 0.41	4.567	0.07 ± 0.07	971 ± 7034	-6.20 ± 10.28	1.305
133	UGC07690	0.10 ± 0.03	5.88 ± 2.02	-2.62 ± 0.47	4.774	0.66 ± 0.49	1.16 ± 1.15	-1.37 ± 1.57	0.703
134	UGC04305	0.21 ± 0.06	5.32 ± 1.65	-2.31 ± 0.42	2.107	2.00 ± 0.30	1.37 ± 0.41	-1.71 ± 0.50	0.691
135	NGC2915	0.27 ± 0.05	5.16 ± 0.70	-2.24 ± 0.20	0.935	0.71 ± 0.25	3.56 ± 0.80	-1.88 ± 0.41	0.703
136	UGC05716	0.27 ± 0.04	7.88 ± 1.72	-2.77 ± 0.31	3.022	0.36 ± 0.10	7.70 ± 1.95	-2.83 ± 0.41	2.627
137	UGC05829	0.32 ± 0.08	8.03 ± 2.71	-2.78 ± 0.48	0.494	0.24 ± 0.37	26.59 ± 43.42	-3.68 ± 2.77	0.119
138	F565-V2	0.31 ± 0.10	7.53 ± 1.83	-2.66 ± 0.34	5.691	1.26 ± 0.51	6.27 ± 15.90	-2.39 ± 4.65	0.250
139	DDO161	0.43 ± 0.06	6.42 ± 1.97	-2.57 ± 0.43	0.530	1.41 ± 0.36	9.61 ± 2.29	-2.98 ± 0.38	0.248
140	DDO170	0.27 ± 0.04	6.20 ± 2.01	-2.66 ± 0.45	6.112	0.51 ± 0.18	6.09 ± 2.40	-2.68 ± 0.62	4.660
141	NGC1705	0.11 ± 0.02	4.08 ± 0.90	-2.21 ± 0.30	0.230	0.14 ± 0.08	1.74 ± 0.96	-1.51 ± 0.87	0.069
142	UGC05721	0.19 ± 0.03	4.10 ± 0.98	-2.11 ± 0.33	1.444	0.58 ± 0.18	1.97 ± 0.75	-1.45 ± 0.53	0.525
143	UGC08837	0.58 ± 0.14	13.66 ± 1.55	-3.23 ± 0.18	3.579	1.60 ± 0.43	63.09 ± 31.96	-2.82 ± 0.92	0.999
144	UGC07603	0.28 ± 0.04	5.68 ± 1.44	-2.46 ± 0.35	1.781	1.08 ± 0.37	2.07 ± 0.92	-1.69 ± 0.72	0.356
145	UGC00891	0.47 ± 0.06	5.22 ± 1.48	-2.33 ± 0.40		1.15 ± 0.45	6.31 ± 4.73	-2.58 ± 1.35	
146	UGC01281	0.47 ± 0.07	9.60 ± 0.83	-2.88 ± 0.15	0.367	1.98 ± 0.48	3.15 ± 4.38	-2.11 ± 2.56	0.033
147	UGC09992	0.14 ± 0.05	5.01 ± 1.87	-2.50 ± 0.52		0.06 ± 0.63	1.65 ± 11.86	-2.40 ± 13.19	
148	D512-2	0.18 ± 0.06	4.74 ± 1.71	-2.58 ± 0.51		1.10 ± 0.51	1.90 ± 13.10	-2.13 ± 12.72	
149	UGC00731	0.28 ± 0.04	5.89 ± 1.48	-2.53 ± 0.35	0.278	0.41 ± 0.13	5.26 ± 1.92	-2.47 ± 0.59	0.129
150	UGC08550	0.18 ± 0.02	6.12 ± 1.96	-2.71 ± 0.44	1.568	0.38 ± 0.16	3.25 ± 1.39	-2.24 ± 0.71	0.884
151	UGC07608	0.30 ± 0.10	6.04 ± 2.10	-2.56 ± 0.49	2.181	1.09 ± 0.49	3.96 ± 14.82	-2.13 ± 6.86	0.270
152	NGC2366	0.40 ± 0.04	8.91 ± 1.00	-2.99 ± 0.17	2.151	1.98 ± 0.19	2.76 ± 0.22	-2.13 ± 0.13	0.247
153	NGC4068	0.36 ± 0.11	8.89 ± 1.83	-2.95 ± 0.29		1.52 ± 0.47	33.88 ± 25.76	-2.49 ± 1.37	
154	UGC05918	0.20 ± 0.05	5.31 ± 1.99	-2.67 ± 0.52	0.427	0.58 ± 0.43	2.84 ± 2.95	-2.32 ± 1.86	0.114
155	D631-7	0.83 ± 0.11	9.43 ± 0.70	-2.81 ± 0.13	1.309	1.95 ± 0.38	5.63 ± 3.61	-2.48 ± 1.18	0.684
156	NGC3109	0.74 ± 0.06	8.62 ± 0.72	-2.68 ± 0.14	0.297	1.13 ± 0.33	5.74 ± 3.50	-2.43 ± 1.11	0.213
157	UGCA281	0.23 ± 0.05	8.63 ± 1.28	-3.06 ± 0.21	2.236	0.77 ± 0.32	0.94 ± 4.74	-1.69 ± 9.26	0.689
158	DDO168	0.65 ± 0.08	6.79 ± 0.76	-2.45 ± 0.17	9.147	1.99 ± 0.20	2.85 ± 0.39	-1.93 ± 0.23	4.972
159	DDO064	0.31 ± 0.08	6.14 ± 2.02	-2.68 ± 0.46	0.811	1.85 ± 0.51	1.84 ± 15.32	-1.86 ± 15.30	0.458
160	PGC51017	0.58 ± 0.16	19.01 ± 3.18	-3.83 ± 0.24		1.90 ± 0.44	1714 ± 3592	-4.94 ± 3.75	
161	UGCA442	0.37 ± 0.04	7.75 ± 1.06	-2.86 ± 0.20	2.831	0.81 ± 0.36	4.36 ± 1.61	-2.42 ± 0.67	1.441
162	UGC07866	0.22 ± 0.07	7.51 ± 1.74	-2.99 ± 0.32	1.031	0.26 ± 0.56	9.25 ± 37.37	-3.35 ± 7.40	0.253
163	UGC07232	0.25 ± 0.09	4.73 ± 0.75	-2.43 ± 0.24		1.34 ± 0.48	20.67 ± 12.56	-1.56 ± 1.09	
164	UGC07559	0.32 ± 0.09	10.32 ± 1.46	-3.28 ± 0.21	2.163	1.80 ± 0.54	1.91 ± 23.29	-2.29 ± 22.47	0.380
165	NGC6789	0.25 ± 0.09	3.42 ± 0.65	-2.04 ± 0.28		0.34 ± 0.51	48.76 ± 28.83	-2.44 ± 1.03	
166	KK98-251	0.49 ± 0.09	5.16 ± 1.84	-2.56 ± 0.50	1.008	1.90 ± 0.51	3.07 ± 27.87	-2.53 ± 16.73	0.342
167	UGC05764	0.49 ± 0.12	2.43 ± 0.46	-1.38 ± 0.29	7.613	0.95 ± 0.15	1.60 ± 0.36	-1.62 ± 0.33	4.022
168	CamB	0.60 ± 0.16	10.12 ± 1.53	-3.25 ± 0.22	4.784	1.81 ± 0.41	63.95 ± 32.46	-2.78 ± 0.91	4.026
169	ESO444-G084	0.34 ± 0.05	4.56 ± 0.92	-2.33 ± 0.28	0.974	0.30 ± 0.15	6.68 ± 4.89	-2.59 ± 1.23	0.495
170	DDO154	0.49 ± 0.04	5.59 ± 0.45	-2.71 ± 0.13	6.029	1.21 ± 0.16	3.44 ± 0.22	-2.35 ± 0.11	0.838
171	UGC07577	0.47 ± 0.13	11.69 ± 1.77	-3.49 ± 0.22	1.569	1.36 ± 0.48	79.42 ± 53.12	-3.27 ± 1.15	0.293
172	D564-8	0.35 ± 0.08	9.28 ± 1.74	-3.32 ± 0.26		1.70 ± 0.51	2.17 ± 20.47	-2.49 ± 17.41	
173	NGC3741	0.40 ± 0.05	6.80 ± 0.61	-2.88 ± 0.14	0.635	0.13 ± 0.11	118.2 ± 232.5	-4.82 ± 2.76	0.444
174	UGC04483	0.23 ± 0.05	5.52 ± 0.90	-3.02 ± 0.23	1.937	0.56 ± 0.24	0.97 ± 4.15	-1.94 ± 7.86	0.973
175	UGCA444	0.29 ± 0.05	5.60 ± 0.61	-2.95 ± 0.17	0.115	0.11 ± 0.19	478 ± 4305	-5.70 ± 12.84	0.063

**Table A2.** Same as Table A2, but for the DC14 profile.

SPARC ID	Galaxy Name	$\log(\frac{m_\star}{M_{\text{halo}}})$	$r_s$ kpc	$\log \rho_s$ [ $M_\odot \text{ pc}^{-3}$ ]	$\chi^2_\nu$	$\log(\frac{m_\star}{M_{\text{halo}}})$	$r_s$ kpc	$\log \rho_s$ [ $M_\odot \text{ pc}^{-3}$ ]	$\chi^2_\nu$
001	UGC02487	-0.97	36.05 ± 9.72	-2.23 ± 0.36	5.532	-0.92	40.82 ± 25.72	-2.23 ± 0.62	5.499
002	UGC02885	-1.45	58.54 ± 13.83	-2.77 ± 0.33	1.005	-1.43	80.95 ± 31.30	-3.01 ± 0.40	1.015
003	NGC6195	-2.10	112.40 ± 21.97	-3.20 ± 0.32	2.148	-1.68	95.51 ± 27.76	-3.25 ± 0.40	2.047
004	UGC11455	-1.77	82.43 ± 15.28	-3.07 ± 0.29	4.829	-1.76	85.45 ± 17.57	-3.10 ± 0.24	4.832
005	NGC5371	-0.94	7.38 ± 1.04	-1.03 ± 0.19	2.904	-0.96	5.32 ± 1.06	-0.73 ± 0.20	2.710
006	NGC2955	-1.30	23.83 ± 6.57	-1.89 ± 0.37	3.399	-1.30	9.78 ± 3.04	-0.92 ± 0.33	2.754
007	NGC0801	-1.05	53.41 ± 14.71	-2.79 ± 0.37	8.979	-1.51	283.4 ± 136.6	-4.15 ± 0.52	6.771
008	ESO563-G021	-1.94	110.58 ± 15.80	-3.10 ± 0.21	17.875	-1.89	113.16 ± 18.77	-3.14 ± 0.19	17.879
009	UGC09133	-1.14	37.26 ± 5.98	-2.41 ± 0.22	7.082	-1.07	47.82 ± 9.36	-2.59 ± 0.21	7.064
010	UGC02953	-1.31	20.59 ± 3.71	-1.77 ± 0.24	5.822	-1.32	15.71 ± 3.00	-1.54 ± 0.20	5.798
011	NGC7331	-1.49	33.34 ± 4.73	-2.50 ± 0.19	0.812	-1.50	30.45 ± 5.20	-2.42 ± 0.18	0.801
012	NGC3992	-1.20	30.00 ± 8.13	-2.13 ± 0.36	1.261	-1.08	17.60 ± 8.02	-1.68 ± 0.45	0.694
013	NGC6674	-2.05	234.24 ± 70.76	-3.81 ± 0.47	1.766	-1.81	381.7 ± 259.9	-4.21 ± 0.73	1.460
014	NGC5985	-1.30	16.04 ± 3.18	-1.43 ± 0.26	2.869	-1.71	2.65 ± 0.54	-0.26 ± 0.21	2.043
015	NGC2841	-1.38	60.37 ± 10.79	-2.76 ± 0.24	1.420	-1.37	71.07 ± 16.02	-2.88 ± 0.23	1.415
016	IC4202	-2.20	1.90 ± 0.10	-0.21 ± 0.07	5.551	-2.26	1.92 ± 0.04	-0.22 ± 0.02	5.076
017	NGC5005	-1.52	40.00 ± 16.74	-2.65 ± 0.69	0.154	-1.68	24.75 ± 14.39	-2.18 ± 0.81	0.092
018	NGC5907	-1.17	14.76 ± 3.09	-1.62 ± 0.27	4.513	-1.24	9.96 ± 1.68	-1.23 ± 0.17	4.077
019	UGC05253	-1.50	6.49 ± 0.95	-1.09 ± 0.22	2.578	-1.61	2.41 ± 0.36	-0.37 ± 0.19	2.004
020	NGC5055	-1.37	8.13 ± 0.83	-1.34 ± 0.14	2.988	-1.39	7.24 ± 0.80	-1.22 ± 0.13	3.031
021	NGC2998	-1.30	23.94 ± 5.09	-2.06 ± 0.28	1.367	-1.30	19.06 ± 7.26	-1.85 ± 0.38	1.202
022	UGC11914	-2.24	36.54 ± 6.60	-2.17 ± 0.29	0.670	-2.59	31.95 ± 5.78	-1.88 ± 0.22	0.605
023	NGC3953	-1.30	28.88 ± 22.45	-2.25 ± 1.37	1.133	-1.01	15.71 ± 26.94	-1.83 ± 1.72	0.699
024	UGC12506	-1.30	23.28 ± 4.67	-1.92 ± 0.27	0.250	-1.34	12.54 ± 3.93	-1.47 ± 0.31	0.189
025	NGC0891	-1.45	11.69 ± 1.64	-1.67 ± 0.19	4.777	-1.45	7.50 ± 1.42	-1.29 ± 0.19	3.738
026	UGC06614	-1.68	44.99 ± 11.01	-2.85 ± 0.35	0.250	-1.68	38.44 ± 16.43	-2.69 ± 0.44	0.197
027	UGC02916	-1.13	2.94 ± 0.42	-0.13 ± 0.21	5.890	-0.26	1.15 ± 0.09	0.53 ± 0.12	3.748
028	UGC03205	-1.29	23.21 ± 6.47	-2.03 ± 0.37	3.203	-1.37	5.62 ± 2.05	-0.89 ± 0.37	3.007
029	NGC5033	-1.37	8.76 ± 1.93	-1.31 ± 0.29	4.505	-1.53	3.38 ± 0.65	-0.65 ± 0.19	3.830
030	NGC4088	-1.72	41.02 ± 13.68	-2.94 ± 0.56	0.628	-2.27	49.85 ± 19.79	-2.82 ± 0.59	0.614
031	NGC4157	-1.70	42.86 ± 11.22	-2.91 ± 0.43	0.452	-1.67	41.95 ± 17.10	-2.89 ± 0.59	0.461
032	UGC03546	-1.36	21.01 ± 5.26	-2.13 ± 0.34	1.132	-1.40	7.26 ± 2.19	-1.27 ± 0.31	1.063
033	UGC06787	-1.86	146.65 ± 68.42	-3.55 ± 0.62	17.836	-1.81	181.45 ± 77.29	-3.72 ± 0.42	17.635
034	NGC4051	-1.35	25.54 ± 17.48	-2.45 ± 1.22	2.256	-0.75	17.66 ± 59.64	-2.29 ± 3.44	2.032
035	NGC4217	-1.65	19.64 ± 4.28	-2.30 ± 0.31	3.081	-1.94	1.31 ± 0.22	-0.11 ± 0.18	1.865
036	NGC3521	-1.73	35.55 ± 8.73	-2.67 ± 0.39	0.244	-1.88	29.17 ± 12.21	-2.47 ± 0.62	0.230
037	NGC2903	-1.45	3.97 ± 0.86	-0.82 ± 0.29	7.024	-1.67	1.31 ± 0.08	0.04 ± 0.08	5.465
038	NGC2683	-1.16	22.88 ± 6.34	-2.22 ± 0.37	2.341	-1.01	8.98 ± 5.54	-1.42 ± 0.61	1.920
039	NGC4013	-1.71	50.21 ± 7.95	-3.05 ± 0.24	0.813	-1.70	50.29 ± 8.58	-3.05 ± 0.20	0.807
040	NGC7814	-1.44	16.41 ± 2.55	-1.95 ± 0.21	0.604	-1.42	11.53 ± 2.29	-1.63 ± 0.20	0.542
041	UGC06786	-1.50	15.37 ± 2.66	-1.89 ± 0.23	0.952	-1.57	7.63 ± 1.40	-1.34 ± 0.19	0.844
042	NGC3877	-1.39	16.31 ± 4.59	-2.13 ± 0.37	7.276	-1.96	1.23 ± 0.24	-0.14 ± 0.21	2.059
043	NGC0289	-1.34	28.19 ± 7.19	-2.48 ± 0.35	2.078	-1.24	46.44 ± 27.24	-2.86 ± 0.59	1.977
044	NGC1090	-1.43	25.89 ± 8.20	-2.56 ± 0.42	3.154	-1.98	1.21 ± 0.13	-0.14 ± 0.12	0.923
045	NGC3726	-1.89	56.42 ± 17.52	-3.16 ± 0.53	2.550	-2.06	61.70 ± 26.80	-3.15 ± 0.66	2.494
046	UGC09037	-1.72	18.79 ± 3.51	-2.44 ± 0.27	1.710	-1.77	12.39 ± 3.41	-2.09 ± 0.29	1.324
047	NGC6946	-1.46	25.55 ± 5.59	-2.55 ± 0.31	1.745	-1.46	20.19 ± 5.04	-2.35 ± 0.27	1.754
048	NGC4100	-1.28	22.11 ± 5.38	-2.18 ± 0.32	1.335	-1.23	16.05 ± 6.77	-1.91 ± 0.42	1.311
049	NGC3893	-1.48	19.10 ± 4.37	-2.27 ± 0.32	1.862	-1.49	9.11 ± 4.98	-1.63 ± 0.55	1.152
050	UGC06973	-1.75	6.33 ± 1.09	-1.44 ± 0.25	4.375	-1.85	3.15 ± 0.91	-0.86 ± 0.33	1.765
051	ESO079-G014	-1.66	28.84 ± 7.86	-2.63 ± 0.38	3.859	-2.28	2.28 ± 0.65	-0.64 ± 0.30	0.950
052	UGC08699	-1.42	28.46 ± 6.22	-2.56 ± 0.31	0.724	-1.42	29.33 ± 9.75	-2.58 ± 0.35	0.723
053	NGC4138	-1.31	20.84 ± 7.31	-2.22 ± 0.55	6.718	-1.03	5.47 ± 5.87	-1.08 ± 1.06	5.267
054	NGC3198	-1.50	10.32 ± 1.86	-1.91 ± 0.24	1.551	-1.62	5.53 ± 1.14	-1.43 ± 0.21	1.242
055	NGC3949	-1.44	19.39 ± 6.07	-2.45 ± 0.46	1.731	-2.71	23.30 ± 11.05	-2.00 ± 0.67	0.852
056	NGC6015	-1.37	22.51 ± 5.41	-2.43 ± 0.32	8.256	-1.37	23.60 ± 10.06	-2.47 ± 0.42	8.259
057	NGC3917	-1.63	33.86 ± 11.19	-2.97 ± 0.54	3.270	-2.19	2.00 ± 0.56	-0.76 ± 0.28	1.518
058	NGC4085	-1.61	12.79 ± 3.41	-2.28 ± 0.37	13.690	-2.05	7.05 ± 6.30	-1.65 ± 1.40	6.989
059	NGC4389	-1.67	13.38 ± 3.79	-2.55 ± 0.39	23.928	-2.70	9.50 ± 4.38	-1.69 ± 0.63	8.280
060	NGC4559	-1.55	14.20 ± 3.81	-2.42 ± 0.36	0.320	-1.64	5.90 ± 2.54	-1.72 ± 0.44	0.212

**Table A2** – *continued*

SPARC ID	Galaxy Name	$\log(\frac{m_\star}{M_{\text{halo}}})$	$r_s$ kpc	$\log \rho_s$ [ $M_\odot \text{pc}^{-3}$ ]	$\chi^2_\nu$	$\log(\frac{m_\star}{M_{\text{halo}}})$	$r_s$ kpc	$\log \rho_s$ [ $M_\odot \text{pc}^{-3}$ ]	$\chi^2_\nu$
061	NGC3769	-1.52	12.73 ± 2.84	-2.30 ± 0.30	1.205	-1.57	7.74 ± 3.00	-1.90 ± 0.39	0.837
062	NGC4010	-1.71	14.48 ± 3.23	-2.39 ± 0.32	2.847	-1.85	9.46 ± 4.77	-2.04 ± 0.71	2.285
063	NGC3972	-1.62	14.04 ± 3.48	-2.33 ± 0.34	2.040	-1.78	6.80 ± 2.70	-1.75 ± 0.50	1.194
064	UGC03580	-1.82	8.82 ± 1.28	-2.08 ± 0.20	2.496	-1.87	6.65 ± 1.09	-1.83 ± 0.18	2.471
065	NGC6503	-1.53	6.66 ± 0.57	-1.78 ± 0.11	1.597	-1.54	5.94 ± 0.54	-1.69 ± 0.09	1.555
066	UGC11557	-1.72	13.35 ± 4.20	-2.62 ± 0.47	1.393	-2.31	4.29 ± 3.70	-1.08 ± 1.17	0.518
067	UGC00128	-1.49	17.35 ± 3.01	-2.56 ± 0.24	3.896	-1.50	16.65 ± 3.83	-2.53 ± 0.24	3.908
068	F579-V1	-1.36	11.61 ± 3.47	-2.10 ± 0.40	0.620	-1.59	3.02 ± 2.03	-0.93 ± 0.73	0.207
069	NGC4183	-1.43	13.26 ± 3.68	-2.35 ± 0.37	0.245	-1.48	7.63 ± 3.65	-1.93 ± 0.47	0.208
070	F571-8	-2.26	6.98 ± 1.07	-1.80 ± 0.21	2.306	-2.62	2.67 ± 0.74	-0.94 ± 0.28	0.480
071	NGC2403	-1.65	6.62 ± 0.36	-1.77 ± 0.08	10.258	-1.65	6.40 ± 0.36	-1.73 ± 0.07	10.247
072	UGC06930	-1.53	12.25 ± 3.45	-2.40 ± 0.38	0.634	-1.61	6.12 ± 3.69	-1.80 ± 0.62	0.330
073	F568-3	-1.84	12.44 ± 3.07	-2.54 ± 0.35	2.582	-2.48	5.58 ± 1.64	-1.30 ± 0.38	1.043
074	UGC01230	-1.56	10.71 ± 3.07	-2.30 ± 0.39	1.683	-2.30	3.57 ± 2.21	-0.98 ± 0.86	0.321
075	NGC0247	-1.59	11.03 ± 2.01	-2.37 ± 0.25	1.892	-1.62	8.93 ± 1.73	-2.22 ± 0.20	1.895
076	NGC7793	-1.64	13.45 ± 2.85	-2.61 ± 0.29	0.892	-1.55	10.82 ± 8.35	-2.42 ± 0.91	0.892
077	UGC06917	-1.65	9.89 ± 2.22	-2.24 ± 0.30	1.028	-1.77	5.18 ± 1.62	-1.74 ± 0.32	0.581
078	NGC1003	-1.75	21.67 ± 3.63	-2.91 ± 0.23	2.640	-1.74	24.31 ± 5.29	-3.00 ± 0.22	2.638
079	F574-1	-1.68	7.84 ± 1.73	-2.10 ± 0.30	1.387	-1.89	4.30 ± 1.69	-1.53 ± 0.43	0.532
080	F568-1	-1.68	9.73 ± 2.35	-2.27 ± 0.33	0.912	-2.10	4.20 ± 1.94	-1.33 ± 0.55	0.221
081	UGC06983	-1.59	8.89 ± 2.09	-2.14 ± 0.31	0.792	-1.74	4.11 ± 1.17	-1.54 ± 0.29	0.580
082	UGC05986	-1.78	9.76 ± 2.99	-2.17 ± 0.42	3.583	-2.36	1.34 ± 0.29	-0.58 ± 0.22	1.305
083	NGC0055	-1.96	7.91 ± 0.87	-2.31 ± 0.15	0.773	-1.99	7.55 ± 0.90	-2.27 ± 0.13	0.705
084	ESO116-G012	-1.80	7.97 ± 1.72	-2.09 ± 0.29	1.447	-2.03	2.96 ± 0.99	-1.29 ± 0.34	0.839
085	UGC07323	-1.79	12.00 ± 3.27	-2.57 ± 0.37	0.578	-1.98	7.84 ± 10.00	-2.17 ± 2.00	0.314
086	UGC05005	-1.88	12.52 ± 3.10	-2.73 ± 0.34	0.137	-2.02	11.91 ± 13.90	-2.58 ± 1.58	0.040
087	F561-1	-1.76	11.06 ± 3.25	-2.56 ± 0.40	3.947	-0.96	9.50 ± 51.41	-2.53 ± 5.87	1.562
088	NGC0024	-1.55	10.18 ± 2.18	-2.22 ± 0.30	0.572	-1.76	1.97 ± 0.44	-0.88 ± 0.22	0.759
089	F568-V1	-1.67	7.41 ± 1.85	-2.09 ± 0.34	0.403	-1.97	3.31 ± 1.96	-1.28 ± 0.72	0.087
090	UGC06628	-1.74	12.69 ± 3.98	-2.66 ± 0.43	2.023	-0.80	2.74 ± 6.42	-1.46 ± 3.01	0.308
091	UGC02455	-2.20	5.19 ± 1.40	-2.15 ± 0.37	7.381	-3.06	1.15 ± 0.49	-0.60 ± 0.57	2.622
092	UGC07089	-1.86	10.69 ± 2.24	-2.58 ± 0.29	0.173	-1.94	10.88 ± 15.68	-2.55 ± 2.29	0.128
093	UGC05999	-1.89	10.16 ± 2.56	-2.57 ± 0.35		-2.48	6.72 ± 4.76	-1.78 ± 1.02	
094	NGC2976	-1.83	11.38 ± 3.31	-2.59 ± 0.39	0.778	-2.51	5.15 ± 2.10	-1.45 ± 0.57	0.398
095	UGC05750	-1.90	10.62 ± 2.57	-2.61 ± 0.33	0.575	-2.03	8.52 ± 4.43	-2.39 ± 0.55	0.428
096	NGC0100	-1.87	9.09 ± 2.13	-2.35 ± 0.32	0.376	-2.05	3.62 ± 2.24	-1.63 ± 0.66	0.176
097	UGC00634	-1.87	10.57 ± 2.53	-2.56 ± 0.33		-2.18	6.47 ± 3.30	-2.01 ± 0.55	
098	F563-V2	-1.73	9.91 ± 2.82	-2.42 ± 0.38	1.221	-2.34	2.54 ± 1.40	-0.90 ± 0.76	0.291
099	NGC5585	-1.90	7.32 ± 1.21	-2.20 ± 0.22	5.819	-1.96	5.30 ± 1.07	-1.93 ± 0.21	5.704
100	NGC0300	-1.79	8.55 ± 2.05	-2.37 ± 0.32	0.573	-1.89	4.91 ± 1.57	-1.83 ± 0.34	0.502
101	UGC06923	-1.81	8.49 ± 1.90	-2.32 ± 0.30	3.998	-1.89	4.74 ± 8.59	-1.85 ± 2.89	2.485
102	F574-2	-1.93	12.19 ± 3.41	-2.78 ± 0.38		-0.27	238 ± 30222	-5.62 ± 128.17	
103	UGC07125	-1.78	7.99 ± 3.11	-2.54 ± 0.52	1.613	-1.81	3.77 ± 1.68	-1.97 ± 0.44	0.269
104	UGC07524	-1.85	5.42 ± 0.75	-2.03 ± 0.19	0.319	-1.87	4.81 ± 0.72	-1.96 ± 0.16	0.265
105	UGC06399	-1.82	7.52 ± 1.61	-2.21 ± 0.29	0.505	-1.95	4.26 ± 1.20	-1.77 ± 0.30	0.294
106	UGC07151	-1.73	11.26 ± 1.91	-2.57 ± 0.24	2.581	-1.62	4.51 ± 1.64	-1.88 ± 0.42	3.506
107	F567-2	-1.91	9.62 ± 2.75	-2.57 ± 0.38		-1.72	4.01 ± 9.18	-1.83 ± 3.21	
108	UGC04325	-1.51	7.36 ± 2.41	-2.03 ± 0.44	6.207	-2.19	0.80 ± 0.16	-0.32 ± 0.23	0.802
109	UGC00191	-1.60	9.17 ± 3.23	-2.32 ± 0.47	4.856	-1.80	2.66 ± 0.88	-1.44 ± 0.35	4.111
110	F563-1	-1.88	7.50 ± 1.72	-2.27 ± 0.31	0.994	-2.39	3.44 ± 1.36	-1.40 ± 0.48	0.683
111	F571-V1	-1.97	8.95 ± 2.23	-2.55 ± 0.34	0.491	-2.07	6.19 ± 7.25	-2.15 ± 1.54	0.183
112	UGC07261	-1.87	12.46 ± 3.84	-2.78 ± 0.42	2.804	-1.54	3.12 ± 4.28	-1.61 ± 1.50	0.192
113	UGC10310	-1.76	9.56 ± 2.96	-2.47 ± 0.42	3.126	-1.85	2.55 ± 2.08	-1.46 ± 0.85	0.612
114	UGC02259	-1.48	7.65 ± 2.40	-2.08 ± 0.42	2.641	-1.63	2.55 ± 1.03	-1.31 ± 0.40	1.783
115	F583-4	-1.89	10.39 ± 2.66	-2.63 ± 0.35	0.528	-1.73	5.63 ± 7.44	-2.20 ± 1.93	0.253
116	UGC12732	-1.73	9.70 ± 2.12	-2.48 ± 0.30	0.316	-1.68	7.87 ± 2.66	-2.41 ± 0.36	0.180
117	UGC06818	-2.11	6.92 ± 1.21	-2.31 ± 0.24	4.143	-2.70	8.37 ± 3.40	-2.16 ± 0.59	2.245
118	UGC04499	-1.81	9.16 ± 2.65	-2.51 ± 0.39	1.962	-2.01	2.53 ± 1.71	-1.52 ± 0.67	0.462
119	F563-V1	-2.20	11.65 ± 3.19	-2.96 ± 0.37	4.856	-0.29	11.2 ± 130.1	-3.48 ± 12.70	1.137
120	UGC06667	-1.94	4.92 ± 0.78	-1.91 ± 0.22	0.544	-2.11	3.24 ± 0.67	-1.58 ± 0.21	0.206



**Table A2** – *continued*

SPARC ID	Galaxy Name	$\log(\frac{m_\star}{M_{\text{halo}}})$	$r_s$ kpc	$\log \rho_s$ [ $M_\odot \text{ pc}^{-3}$ ]	$\chi^2_\nu$	$\log(\frac{m_\star}{M_{\text{halo}}})$	$r_s$ kpc	$\log \rho_s$ [ $M_\odot \text{ pc}^{-3}$ ]	$\chi^2_\nu$
121	UGC02023	-2.08	9.30 ± 2.66	-2.65 ± 0.39		-2.74	7.13 ± 9.38	-1.93 ± 1.73	
122	UGC04278	-2.05	7.97 ± 1.40	-2.31 ± 0.24	0.845	-3.48	23.59 ± 12.69	-2.42 ± 0.61	0.506
123	UGC12632	-1.84	5.48 ± 1.35	-2.10 ± 0.33	0.457	-1.91	2.96 ± 1.54	-1.68 ± 0.51	0.092
124	UGC08286	-1.96	2.10 ± 0.34	-1.25 ± 0.21	1.578	-1.98	1.89 ± 0.19	-1.17 ± 0.10	1.399
125	UGC07399	-1.74	5.70 ± 1.24	-1.89 ± 0.29	1.238	-2.00	1.89 ± 0.65	-1.01 ± 0.34	0.863
126	NGC4214	-2.10	6.96 ± 1.09	-2.41 ± 0.22	1.328	-1.73	3.63 ± 5.23	-1.90 ± 1.94	1.088
127	UGC05414	-2.00	8.73 ± 2.07	-2.52 ± 0.32	0.583	-2.03	4.75 ± 6.86	-2.06 ± 2.21	0.424
128	UGC08490	-1.64	6.06 ± 1.70	-2.10 ± 0.37	0.348	-1.75	1.95 ± 0.46	-1.19 ± 0.24	0.150
129	IC2574	-2.33	9.69 ± 0.75	-2.68 ± 0.12	2.443	-3.14	22.47 ± 3.23	-2.84 ± 0.19	2.171
130	UGC06446	-1.72	6.49 ± 1.87	-2.15 ± 0.39	0.611	-1.84	2.74 ± 1.09	-1.50 ± 0.40	0.287
131	F583-1	-2.13	5.68 ± 1.00	-2.14 ± 0.24	0.390	-2.42	3.51 ± 1.05	-1.70 ± 0.31	0.184
132	UGC11820	-1.84	13.50 ± 2.81	-2.86 ± 0.29	2.873	-1.77	17.80 ± 6.41	-3.14 ± 0.40	2.534
133	UGC07690	-1.98	11.68 ± 2.62	-2.80 ± 0.31	2.045	-1.47	1.19 ± 0.85	-0.89 ± 0.75	0.940
134	UGC04305	-2.10	17.20 ± 3.70	-3.24 ± 0.29	2.119	-2.38	1.05 ± 0.39	-0.43 ± 0.49	0.924
135	NGC2915	-2.26	2.47 ± 0.30	-1.43 ± 0.16	0.758	-2.39	1.85 ± 0.27	-1.13 ± 0.16	0.526
136	UGC05716	-1.86	6.60 ± 0.96	-2.29 ± 0.21	2.433	-1.79	5.48 ± 1.02	-2.32 ± 0.21	2.123
137	UGC05829	-2.10	7.12 ± 1.80	-2.44 ± 0.35	0.513	-4.93	1270 ± 22004	-4.83 ± 17.58	0.128
138	F565-V2	-2.19	6.22 ± 1.22	-2.31 ± 0.27	0.423	-2.60	4.42 ± 4.32	-1.88 ± 1.50	0.127
139	DDO161	-2.30	7.39 ± 1.34	-2.57 ± 0.25	0.257	-2.33	6.91 ± 1.84	-2.51 ± 0.27	0.250
140	DDO170	-2.19	4.65 ± 1.03	-2.16 ± 0.31	3.184	-2.38	2.57 ± 1.27	-1.73 ± 0.49	2.469
141	NGC1705	-1.88	4.23 ± 0.70	-1.82 ± 0.23	0.905	-1.79	0.79 ± 0.17	-0.47 ± 0.22	0.388
142	UGC05721	-1.84	3.29 ± 0.81	-1.61 ± 0.33	1.012	-2.09	1.04 ± 0.27	-0.68 ± 0.26	0.441
143	UGC08837	-2.37	6.15 ± 0.77	-2.42 ± 0.18	1.647	-2.71	7.72 ± 2.31	-2.39 ± 0.44	1.182
144	UGC07603	-2.03	6.04 ± 1.28	-2.26 ± 0.29	1.558	-2.28	1.13 ± 0.41	-0.97 ± 0.36	0.268
145	UGC00891	-2.32	6.68 ± 1.32	-2.45 ± 0.27		-2.51	4.43 ± 1.85	-2.08 ± 0.43	
146	UGC01281	-2.40	3.62 ± 0.38	-1.93 ± 0.16	0.216	-2.33	3.07 ± 1.15	-1.84 ± 0.58	0.165
147	UGC09992	-2.40	8.65 ± 2.38	-2.80 ± 0.38		-1.08	1.39 ± 3.59	-1.31 ± 3.65	
148	D512-2	-2.23	8.25 ± 2.19	-2.67 ± 0.36		-1.74	2.53 ± 8.43	-1.99 ± 5.23	
149	UGC00731	-2.16	3.40 ± 0.52	-1.87 ± 0.21	0.684	-2.05	2.94 ± 1.06	-1.78 ± 0.35	0.281
150	UGC08550	-1.95	9.42 ± 1.61	-2.68 ± 0.24	1.621	-1.90	1.88 ± 0.73	-1.50 ± 0.39	0.822
151	UGC07608	-2.34	6.41 ± 1.77	-2.48 ± 0.37	0.831	-2.54	2.64 ± 2.88	-1.60 ± 1.63	0.178
152	NGC2366	-2.47	2.40 ± 0.25	-1.74 ± 0.15	0.877	-2.36	2.22 ± 0.25	-1.75 ± 0.13	0.781
153	NGC4068	-2.50	4.92 ± 1.00	-2.31 ± 0.28	2.088	-2.76	4.49 ± 2.62	-2.04 ± 0.85	1.259
154	UGC05918	-2.27	6.34 ± 1.85	-2.47 ± 0.39	4.396	-1.89	1.95 ± 1.53	-1.74 ± 0.84	0.082
155	D631-7	-2.71	4.31 ± 0.31	-2.13 ± 0.11	2.052	-2.98	5.68 ± 0.83	-2.18 ± 0.20	1.431
156	NGC3109	-2.59	4.02 ± 0.29	-1.99 ± 0.11	0.290	-2.88	4.50 ± 0.61	-1.96 ± 0.19	0.194
157	UGCA281	-2.32	3.74 ± 0.73	-1.95 ± 0.27	1.521	-1.74	1.38 ± 6.15	-1.52 ± 7.21	0.848
158	DDO168	-2.60	2.95 ± 0.29	-1.79 ± 0.14	7.005	-2.73	2.79 ± 0.42	-1.65 ± 0.20	6.119
159	DDO064	-2.36	5.18 ± 1.26	-2.28 ± 0.33	0.613	-2.35	1.77 ± 2.23	-1.54 ± 1.96	0.413
160	PGC51017	-2.66	11.04 ± 1.99	-3.17 ± 0.25	12.634	-0.71	4.60 ± 12.08	-3.10 ± 4.07	7.186
161	UGCA442	-2.61	2.80 ± 0.29	-1.85 ± 0.15	1.367	-2.58	2.54 ± 0.35	-1.76 ± 0.16	1.119
162	UGC07866	-2.62	4.65 ± 0.89	-2.31 ± 0.26	1.261	-1.78	1.67 ± 7.74	-1.86 ± 7.50	0.108
163	UGC07232	-2.50	5.23 ± 3.11	-2.37 ± 0.78		-2.81	1.33 ± 0.71	-0.98 ± 0.79	
164	UGC07559	-2.69	4.33 ± 0.62	-2.27 ± 0.20	0.922	-2.16	2.39 ± 4.13	-2.10 ± 2.76	0.360
165	NGC6789	-2.48	6.41 ± 3.32	-2.56 ± 0.68		-3.11	1.17 ± 0.61	-0.57 ± 0.72	
166	KK98-251	-2.65	5.96 ± 1.41	-2.57 ± 0.32	0.397	-2.48	3.41 ± 2.30	-2.28 ± 0.94	0.399
167	UGC05764	-2.46	1.55 ± 0.22	-1.23 ± 0.20	4.245	-2.47	0.93 ± 0.33	-0.96 ± 0.49	4.051
168	CamB	-2.93	5.02 ± 0.78	-2.54 ± 0.22	4.371	-2.71	3.88 ± 1.35	-2.48 ± 0.49	4.255
169	ESO444-G084	-2.64	2.81 ± 0.67	-1.89 ± 0.32	5.044	-4.10	32.76 ± 32.92	-2.96 ± 1.51	1.949
170	DDO154	-2.87	2.51 ± 0.14	-1.86 ± 0.08	1.621	-2.84	2.44 ± 0.14	-1.84 ± 0.07	1.655
171	UGC07577	-2.97	6.14 ± 1.08	-2.73 ± 0.24	0.289	-2.71	5.43 ± 4.02	-2.81 ± 1.10	0.232
172	D564-8	-3.01	4.44 ± 0.57	-2.44 ± 0.19	2.976	-2.38	1.98 ± 1.75	-2.17 ± 1.37	0.332
173	NGC3741	-3.01	2.88 ± 0.23	-1.93 ± 0.12	0.871	-4.11	31.55 ± 15.48	-3.22 ± 0.70	0.430
174	UGC04483	-3.22	2.79 ± 0.38	-1.99 ± 0.20	3.645	-2.23	0.51 ± 4.29	-1.19 ± 13.61	0.510
175	UGCA444	-3.36	2.45 ± 0.28	-1.87 ± 0.17	0.171	-6.49	1571 ± 4891	-5.01 ± 3.17	0.065